Journal of Environmental Management 341 (2023) 118109

Contents lists available at ScienceDirect

Journal of Environmental Management

journal homepage: www.elsevier.com/locate/jenvman

Research article

Effect of common ions aging treatment on adsorption of phosphate onto and control of phosphorus release from sediment by lanthanum-modified bentonite

Yanhui Zhan, Bo Qiu, Jianwei Lin *

College of Marine Ecology and Environment, Shanghai Ocean University, Shanghai, 201306, China

ARTICLE INFO

Keywords:
Lanthanum-modified bentonite
Combined aging treatment
Sediment
Phosphorus
Addition
Capping

ABSTRACT

The objective of this work was to explore the influence of combined aging treatment using Na^+, Ca^{2+}, Cl^-, HCO_3^- and SO_4^{2-} on the adsorption of phosphate ($H_iPO_4^{i-3}$) onto and the restraint of internal phosphorus (P) migration into overlying water (OW) by lanthanum modified bentonite (LMB). To achieve this aim, the adsorption characteristics and mechanisms of $H_iPO_4^{i-3}$ onto the raw and aged LMBs (named as R-LMB and A-LMB, respectively) were comparatively studied, and the effects of R-LMB and A-LMB treatments (addition and capping) on the migration of P from sediment to OW were comparatively investigated. The results showed that the combined aging treatment of R-LMB with Na^+, Ca^{2+}, Cl^-, HCO_3^- and SO_4^{2-} inhibited the adsorption of $H_iPO_4^{i-3}$. Similar to R-LMB, the precipitation of $H_iPO_4^{i-3}$ with La^{3+} to form $LaPO_4$ and the ligand exchange between CO_3^{2-} and $H_iPO_4^{i-3}$ to form the inner-sphere lanthanum-phosphate complexes are the important mechanisms for the $H_iPO_4^{i-3}$ uptake by A-LMB. The R-LMB addition and capping can be effective in the suppression of endogenous P release to OW under hypoxia conditions. The inactivation of diffusive gradient in thin film-unstable P (DGT-UP) and potentially mobile P (PM-P) in sediment acted as a key role in the restraint of internal P release to OW by the R-LMB addition, and the immobilization of DGT-UP and PM-P in the topmost sediment played a key role in the interception of endogenous P migration into OW by the R-LMB capping. Although the $Na^+/Ca^{2+}/Cl^-/HCO_3^-/SO_4^{2-}$ combined aging treatment had a certain negative effect on the efficiencies of LMB addition and capping to hinder the liberation of P from sediment into OW, the A-LMB addition and capping still can be effective in the control of sediment internal phosphorus pollution to a certain degree. The results of this work indicate that LMB has a high potential to be used as a capping/amendment material to control internal phosphorus pollution.

1. Introduction

Eutrophication of freshwater bodies such as lake and reservoir, featured with harmful algae overgrowth, remains a serious environmental issue of global significance (Li et al., 2021; Yu et al., 2022; Zang et al., 2022). Phosphorus (P) is commonly regarded as a limiting factor for the freshwater eutrophication (Schindler et al., 2008, 2016; Sills and Schelske, 2009). Therefore, the reduction in the input of P is generally a significant method for the control of the freshwater eutrophication. The reduction in the external P loading is an important strategy for reducing the phosphorus concentration in the overlying water (OW)(Van Heyst et al., 2022; Xu et al., 2020). However, after the significant reduction in the external phosphorus pollution, the restraint of internal phosphorus release from sediments is critical to the decline in the P concentration of OW (Paytan et al., 2017; Sondergaard et al., 2003; Watson et al., 2016; Yang et al., 2020).

Several measures have been developed to mitigate the release of internal P to OW, including dredging (Yang et al., 2023), aeration or oxygenation (Chen et al., 2021; Wang et al., 2020), nitrate injection (Lin et al., 2021), aluminum salt treatment (Yang et al., 2022), ferric salt treatment (Li et al., 2020), aquatic vegetation reconstruction (Sun et al., 2022), in-situ physical capping (Jiao et al., 2020) and in-situ sorbent immobilization (Copetti et al., 2016; Yin et al., 2016b, 2018). Among them, the in-situ sorbent immobilization has suggested to be an effective approach for the control of internal P pollution (Copetti et al., 2016; Yin et al., 2016b, 2018). It should be noted that there are two basic modes for the in-situ sorbent immobilization technology (Zhan et al., 2020). One is the capping treatment (Zhan et al., 2020). The other is the

* Corresponding author.
E-mail address: jwlin@shou.edu.cn (J. Lin).

https://doi.org/10.1016/j.jenvman.2023.118109
Received 3 March 2023; Received in revised form 21 April 2023; Accepted 4 May 2023
Available online 10 May 2023

amendment treatment (Zhan et al., 2020). The capping treatment, by spraying the P immobilizing sorbent (PIS) onto the OW-sediment interface, can form a barrier layer on the surface sediment and effectively hinder P from entering OW (Zhang et al., 2021). The amendment treatment, by the addition of PIS into sediment, can inactivate P in the sediment and prevent the release of internal P into OW (Zhan et al., 2020). Many PISs have been proposed to limit the internal P release to OW, including lanthanum-based PISs (Kong et al., 2020; Li et al., 2023; Lürling and Oosterhout, 2013), aluminum-based PISs (Gibbs and Özkundakci, 2011; Gibbs et al., 2011; Kuster et al., 2023; Zhang et al., 2021), iron-based PISs (Fuchs et al., 2018; Funes et al., 2017; Xia et al., 2023), calcium-based PISs (Yin and Kong, 2015; Yin et al., 2013; Zhou et al., 2021) and zirconium-based PISs (Yang et al., 2015; Zhan et al., 2020). Amongst them, lanthanum-based PIS is considered as a very promising capping or amendment material to restrain the endogenous P release to OW (Copetti et al., 2016; Li et al., 2019; Wu et al., 2022; Zhan et al., 2021).

Lanthanum modified bentonite (LMB), which is commercially named as Phoslock®, is a broadly used lanthanum-based PIS (La-PIS) for P inactivation in sediment and internal P release control. Knowing the performances and mechanisms of phosphate ($HiPO_4^{i-3}$, $i = 0$, 1, 2 or 3) adsorption onto LMB and internal P release control by LMB is crucial to the practical utilization of LMB to control the internal P pollution. Up to now, the abilities and mechanisms for the adsorption of $H_iPO_4^{i-3}$ onto and the restraint of endogenous P liberation by LMB have been extensively studied (Copetti et al., 2016; Dithmer et al., 2015; He et al., 2022; Kang et al., 2022; Kurzbaum and Bar Shalom, 2016; Lürling et al., 2014; Meis et al., 2012; Reitzel et al., 2013; Ross et al., 2008; Wang et al., 2017; Zamparas et al., 2015). It is worth noting that Na^+, Ca^{2+}, Cl^-, HCO_3^- and SO_4^{2-} extensively exist in natural freshwater bodies (DeVilbiss et al., 2022; Flower et al., 2022). Mucci et al. found that the sodium, calcium and magnesium present in the seawater can replace the lanthanum present in the interlayer of bentonite clay and the carbonate complex such as lanthanite ($La_2(CO_3)_3{\cdot}8H_2O$) or kozoite ($LaCO_3OH$) is possibly formed (Mucci et al., 2020). This has the potential to change the physical behavior of the bentonite (Mucci et al., 2020). Thus, the combined aging treatment of LMB with Na^+, Ca^{2+}, Cl^-, HCO_3^- and SO_4^{2-} in freshwater may alter the physicochemical properties of LMB and thus affect the ability and mechanism of LMB to adsorb $H_iPO_4^{i-3}$ from water and to control internal P pollution. Knowing the effect of common ions aging treatment on adsorption of phosphate onto and control of phosphorus release from sediment by LMB is vital to the application of LMB to control P release from sediment. However, little is known about the effect of Na^+, Ca^{2+}, Cl^-, HCO_3^- and SO_4^{2-} combined aging treatment on the adsorption of $H_iPO_4^{i-3}$ onto and the control of endogenous P release by LMB.

In this study, the raw and $Na^+/Ca^{2+}/Cl^-/HCO_3^-/SO_4^{2-}$ co-treated LMBs (hereafter named as R-LMB and A-LMB) were selected as capping and amendment materials to limit endogenous P liberation. This work aimed to investigate the influence of Na^+, Ca^{2+}, Cl^-, HCO_3^- and SO_4^{2-} combined aging treatment on the adsorption of $H_iPO_4^{i-3}$ onto and the inhibition of internal phosphorus release to OW by LMB. To accomplish this objective, the adsorption characteristics and mechanisms of $H_iPO_4^{i-3}$ onto R-LMB and A-LMB were comparatively studied, and the impact of R-LMB and A-LMB on the migration of internal P from sediment to OW was comparatively explored. The results of this study will provide a technical support for the utilization of LMB in the restoration of eutrophic freshwater bodies.

2. Materials and methods

2.1. Materials

The chemicals utilized in this work were supplied by Sinopharm Chemical Co., Ltd. (Shanghai, China), and were of analytical grade. The sediment and OW were acquired from a landscape freshwater body located in Pudong New Area, Shanghai, China. Prior to use, the sampled sediment was homogenized and passed through the sieve with 20 meshes. The R-LMB applied in this work was supplied by Beijing Linze Shengtai Environmental Technology Development Co., Ltd., China. The flat plate high resolution diffusive gradient in thin-film device (DGT) based on ZrO-Chelex binding gels used in this study was provided by Zhongke Zhigan (Nanjing) Environmental Technology Co., Ltd., China. The stock solution of KH_2PO_4 was prepared by the addition of KH_2PO_4 in deionized water (DW).

2.2. Preparation of A-LMB

A-LMB was synthesized by shaking 2 g of R-LMB in 2 L of NaCl/$CaCl_2$/$NaHCO_3$/Na_2SO_4 mixed solution containing 14 mmol/L of Na^+, 2 mmol/L of Ca^{2+}, 14 mmol/L of Cl^-, 2 mmol/L of HCO_3^- and 1 mmol/L SO_4^{2-} (pH 7) at 150 rpm and 25 °C. After 24 h of reaction, the produced A-LMB was collected by centrifugation and dried in a 105 °C oven.

2.3. Characterization of R-LMB and A-LMB

The crystal phases of R-LMB and A-LMB were characterized by X-ray diffractometer (SMARTLAB9, RIKEN, Japan). A surface area and pore size analyzer (Tristar II 3020, Micromerics, USA) was used to analyze the surface areas and pore structures of R-LMB and A-LMB. The chemical compositions of R-LMB and A-LMB were characterized by wavelength dispersion X-ray fluorescence (XRF) instrument (XRF-1800, SHIMADZU Corporation, Japan). The X-ray photoelectron spectroscopy (XPS) data of R-LMB and A-LMB samples before and after $H_iPO_4^{i-3}$ uptake were acquired by an X-ray photoelectron spectrometer (ESCALAB250Xi, Thermo Fisher Scientific, USA).

2.4. Adsorption experiment

To explore the influence of common ions aging treatment on the adsorption of $H_iPO_4^{i-3}$ onto LMB, the adsorption characteristics of $H_iPO_4^{i-3}$ by R-LMB and A-LMB were comparatively studied using batch experiments. The $H_iPO_4^{i-3}$ working solution was prepared by the dilution of KH_2PO_4 stock solution with DW. The reaction system was shaken in a constant temperature oscillator at 25 °C and 150 rpm. After reaction, the clear solution was acquired from the reaction system through centrifugation followed by filtration (0.45-μm cellulose membrane). The residual concentration of phosphate in the clear filtrate solution was analyzed using the ammonium molybdate spectrophotometric approach. In the pH effect experiment, the final pH of solution was determined using a pH meter. Two repeated experiments were implemented under each experimental condition. This information will not be repeated below.

In the adsorption kinetics experiment, 25 mg of R-LMB or A-LMB was added into 25 mL of 10 mg P/L $H_iPO_4^{i-3}$ solution with initial pH of 7, and the reaction was ended after 0.25, 0.5, 0.75, 1, 2, 4, 6, 16, 24 and 48 h, respectively. To explore the effect of initial phosphorus concentration, 25 mg of R-LMB or A-LMB was added to 25 mL of $H_iPO_4^{i-3}$ solutions with different initial concentrations (R-LMB: 2, 5, 8, 10 and 15 mg P/L; A-LMB: 2, 5, 8, 10 and 20 mg P/L), respectively, and the above mixture solution was shaken for 24 h. To study the impact of adsorbent dosage, a certain mass of R-LMB or A-LMB (5, 10, 15, 20 or 30 mg) was mixed with 25 mL of $H_iPO_4^{i-3}$ solution with an initial pH of 7 and an initial phosphorus concentration of 10 mg/L, and the contact time was set at 1440 min. To investigate the influence of pH, 25 mg of R-LMB or A-LMB was introduced into 25 mL of 10 mg P/L $H_iPO_4^{i-3}$ solutions with initial pH values of 5, 6, 7, 8, 9 and 10, respectively, and the reaction time was 24 h. To make an investigation on the effect of coexisting common anions and cations, 25 mg of R-LMB or A-LMB was shaken in 25 mL of 10 mg P/L $H_iPO_4^{i-3}$ solutions with 0 and 2 mmol/L of coexisting electrolyte (NaCl, $CaCl_2$, Na_2SO_4, $NaHCO_3$, KCl and $MgCl_2$) for 1440 min, respectively.

The mean adsorption rates of R-LMB and A-LMB ($\bar{r}$, mg/g min) were calculated as follows:

$$\overline{r} = \frac{q_{t_2} - q_{t_1}}{\Delta t} \quad (1)$$

where q_{t_2} and q_{t_1} represent the amounts of $H_iPO_4^{i-3}$ adsorbed onto R-LMB or A-LMB at time t_2 and t_1, respectively (mg/g); Δt (min) represents the time interval between t_2 and t_1, and it equals to $t_2 - t_1$.

The obtained kinetics data were simulated using the quasi first order (QFO), quasi second order (QSO) and Elovich equations as follows (Jiang et al., 2021; Khnifira et al., 2023; Tran et al., 2017).

$$q_t = q_e\left(1 - e^{-K_1 t}\right) \quad (2)$$

$$q_t = \frac{K_2 q_e^2 t}{1 + K_2 q_e t} \quad (3)$$

$$q_t = \frac{1}{\beta}(1 + \alpha\beta t) \quad (4)$$

$$r_0 = K_2 q_e^2 \quad (5)$$

where q_t indicates the quantity of $H_iPO_4^{i-3}$ adsorbed by R-LMB or A-LMB (mg P/g) at time t (min); q_e indicates the amount of $H_iPO_4^{i-3}$ adsorbed by R-LMB or A-LMB (mg P/g) in equilibrium state; K_1 is the parameter of the QFO equation (1/min); K_2 is the parameter of the QSO equation (g/mg min); α (mg/g min) and β (g/mg) represent the parameters of the Elovich equation; r_0 (mg/g min) denotes the rate of $H_iPO_4^{i-3}$ adsorption by R-LMB or A-LMB at the initial time.

The obtained isotherms of $H_iPO_4^{i-3}$ adsorption by R-LMB or A-LMB were simulated by the Langmuir and Freundlich equations as follows (Yang et al., 2022a).

$$q_e = \frac{q_s k_L C_e}{1 + k_L C_e} \quad (6)$$

$$q_e = k_F C_e^{\frac{1}{n}} \quad (7)$$

where q_e denotes the quantity of $H_iPO_4^{i-3}$ adsorbed by R-LMB or A-LMB at equilibrium (mg/g); C_e represents the $H_iPO_4^{i-3}$ concentration of solution when reaction arrived at equilibrium (mg/L); q_s is the saturation monolayer adsorption capacity of $H_iPO_4^{i-3}$ (mg/g); k_L (L/mg) and k_F represent the constants of Langmuir and Freundlich equations, respectively.

2.5. Sediment incubation experiment

Sediment incubation experiments were set up to make an evaluation on the influence of common ions aging treatment on the interception of endogenous phosphorus liberation to OW by LMB. We selected 10 cylindrical transparent glass containers with 5 cm in internal radium and 25 cm in height as sediment incubation reactors. The homogenized sediment was utilized to construct the sediment core with 10 cm in height. Five types of sediment incubation groups were established, including the control, R-LMB addition, A-LMB addition, R-LMB capping and A-LMB capping groups. Each group was carried out in duplicate. The sediment core without any treatment was employed as the control group. For the addition group, 4 g of R-LMB or A-LMB was completely mixed with the sediment core. For the capping group, 4 g of R-LMB or A-LMB was evenly sprayed on the surface sediment. By the catalytic oxidation of sodium sulfite (Kim et al., 2003), the OW sample was controlled in anoxia state (dissolved oxygen (DO) < 0.5 mg/L). The anoxic OW was then added to the column until the space above the sediment (control or addition group) or capping material (capping group) was full of water. During the whole period of sediment incubation, each column was closed to avoid oxygenation, and its OW was controlled in anoxic state. During the incubation, we measured the pH, soluble reactive phosphorus (SRP) and dissolved total phosphorus (DTP) of OW regularly. The pH value of OW was determined using a pH meter. The SRP concentration of OW was determined using the molybdenum blue approach. The DTP concentration of OW was determined using the molybdenum blue approach after the potassium persulfate digestion. On the 252nd day, the ZrO-Chelex DGT probe was used to measure the concentrations of DGT-unstable phosphorus and iron (named as DGT-UP and DGT-UF, respectively) in the profile of OW and sediment. The ZrO-Chelex DGT was promptly inserted into the sediment for each group. After 24 h, all the ZrO-Chelex DGT devices were quickly retrieved from the sediment cores. Then, a ceramic blade was utilized to cut the ZrO-Chelex binding gels at 2-mm intervals. After that, each slice was sequentially immersed in 1 mol/L sodium hydroxide solution for phosphorus extraction and 1 mol/L hydrogen nitrate solution for iron extraction (Zheng et al., 2023). The concentrations of phosphorus and iron in the extracting solution were measured using the molybdenum blue and phenanthroline colorimetry approaches, respectively (Lin et al., 2022). The concentrations of DGT-UP and DGT-UF (c_{DGT}, mg/L) in water and sediment were calculated as follows (Zhang et al., 1995, 1998).

$$M = \frac{c_e\left(V_e + V_g\right)}{E} \quad (8)$$

$$c_{DGT} = \frac{M\Delta g}{DAt} \quad (9)$$

where M (μg) indicates the accumulated mass over the time of deployment; c_e (mg/L) represents the phosphorus or iron concentration in the extracting solution; V_e (mL) represents the volume of the extracting solution; V_g (mL) represents the volume of the binding gel; E is the efficiency of extraction; D (cm^2/s) represents the diffusive coefficient of phosphorus or iron in the diffusion layer; A (cm^2) indicates the area of the binding gel exposed to the environment; t (s) represents the time of deployment.

After the incubation experiment, the sediment was sampled to make an analysis on the loosely bound P (LB-P), reductant-soluble P (Fe–P) and potentially mobile P (PM-P). The procedures for the determination of LB-P and Fe–P in the sediment were according to the sequential extraction scheme described in the previous literature (Rydin and Welch, 1998). The content of PM-P in sediment was computed as the total amount of LB-P and Fe–P (Kuster et al., 2023).

In order to make an evaluation on the phosphorus stability in the R-LMB or A-LMB capping layer, the P forms of the R-LMB or A-LMB after its application were analyzed by the sequential extraction procedure described in the previous literatures (Kuster et al., 2023; Rydin and Welch, 1998). The sediment core in the incubation system was set up by adding 20 g of air-dried sediment into 250 mL brown bottle. Then, the permeable fabric-wrapped R-LMB and A-LMB systems were placed onto the surface sediment, respectively. After that, the anoxic OW was added until the space above the capping layer was filled with water. After 247 days of incubation, the R-LMB and A-LMB were collected from the bottles. Afterwards, the quantities of LB-P, Fe–P, metal oxide bound P (NaOH-SRP), calcium bound P (Ca–P) and residual P (Res-P) in the collected R-LMB and A-LMB were determined using 1 mol/L NH_4Cl, 0.11 mol/L $Na_2S_2O_4$/$NaHCO_3$, 0.1 mol/L NaOH, 0.5 mol/L HCl and 1 mol/L NaOH solutions as extractants, respectively (Kuster et al., 2023; Rydin and Welch, 1998). The amount of total P (TP) was computed as the total quantity of LB-P, Fe–P, NaOH-SRP, Ca–P and Res-P.

3. Results and discussion

3.1. Characterization of R-LMB and A-LMB

The XRD patterns of R-LMB and A-LMB are presented in Fig. 1. As depicted in Fig. 1a, the R-LMB sample contained montmorillonite, quartz, feldspars and lanthanum carbonate octahydrate. The change in the $d_{(001)}$ basal spacing between montmorillonite layers can be used to reflect the structural change of montmorillonite (Lin et al., 2016). The

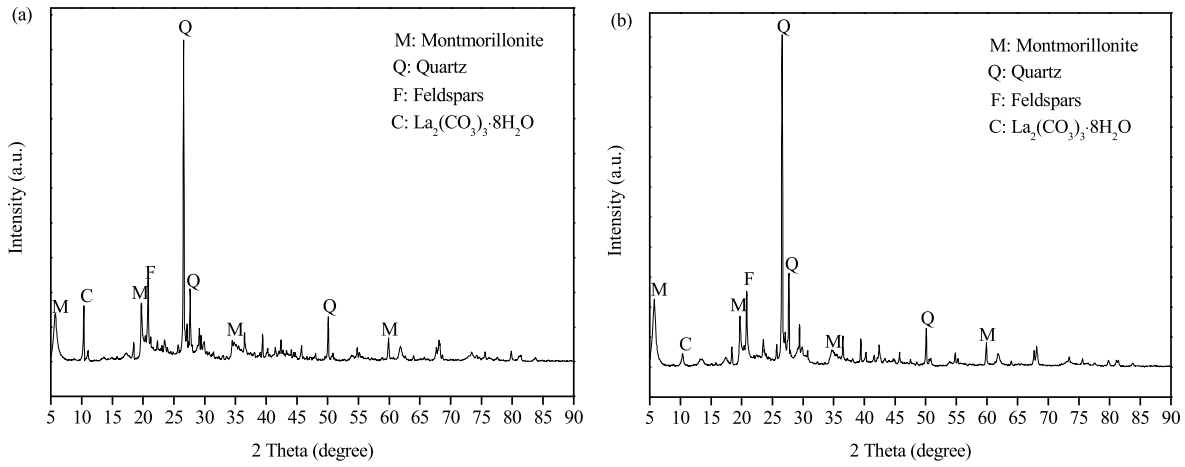

（a）R-LMB；（b）A-LMB

Fig. 1. XRD patterns of R-LMB and A-LMB.

$d_{(001)}$ peak of montmorillonite in the unmodified bentonite occurred at $2\theta = 6.78°$ (Lin et al., 2016). However, the $d_{(001)}$ peak of montmorillonite in the R-LMB sample occurred at $2\theta = 5.72°$. This suggests that lanthanum species has been moved into the interlayers of the montmorillonite mineral after the modification of bentonite with lanthanum. The presence of lanthanum carbonate octahydrate in the R-LMB sample indicates that the lanthanum in the R-LMB can also exist in the form of lanthanum carbonate in addition to La^{3+} (He et al., 2022; Mucci et al., 2020). Similar to the R-LMB sample, the A-LMB sample also included montmorillonite, quartz, feldspars and lanthanum carbonate octahydrate. This demonstrates that in addition to La^{3+}, lanthanum carbonate also is the existing form of lanthanum in the A-LMB sample. The chemical compositions of R-LMB and A-LMB determined by XRF are summarized in Table 1. It was shown that the relative amount of lanthanum in the A-LMB samples (1.043%) was slightly higher that in the R-LMB sample (0.951%). Furthermore, the relative amount of sodium in the A-LMB sample (0.599%) was obviously less than that in the R-LMB sample (1.059%), but the former (2.799%) had a significantly higher relative amount of calcium than the latter (2.035%). This indicates that after the contact of R-LMB with $Na^+/Ca^{2+}/Cl^-/HCO_3^-/SO_4^{2-}$ mixed solution, the cation exchange reaction between the calcium ion in the solution and the sodium ion in the R-LMB takes place, resulting in the fact that the content of calcium in the LMB increases but the content of sodium in the LMB decreases. The Brunauer-Emmett-Teller (BET) specific areas of R-LMB and A-LMB were found to be 7.14 and 12.8 m^2/g, respectively. The total pore volumes of R-LMB and A-LMB were found to be 0.00195 and 0.00349 cm^3/g, respectively. The average pore sizes of R-LMB and A-LMB were determined to be 22.9 and 17.1 nm, respectively. Clearly, A-LMB has higher BET specific surface area and total pore volume than R-LMB.

Table 1
Chemical compositions (wt.%) of R-LMB and A-LMB determined by XRF.

Compounds	R-LMB	A-LMB
Na_2O	1.059	0.599
MgO	2.680	2.456
Al_2O_3	17.295	16.915
SiO_2	69.534	70.875
P_2O_5	0.042	0.045
SO_3	0.059	0.067
Cl	1.048	0.162
K_2O	2.500	2.512
CaO	2.035	2.799
TiO_2	0.275	0.287
MnO	0.055	0.036
Fe_2O_3	2.272	2.159
NiO	0.009	0.000
ZnO	0.009	0.008
Rb_2O	0.010	0.008
SrO	0.012	0.008
Y_2O_3	0.142	0.003
ZrO_2	0.014	0.016
La_2O_3	0.951	1.043

3.2. Adsorption of phosphate on R-LMB and A-LMB

3.2.1. Adsorption kinetics

The adsorption kinetic curve of $H_iPO_4^{i-3}$ by R-LMB and A-LMB is displayed in Fig. 2a. The average rates of $H_iPO_4^{i-3}$ adsorption onto R-LMB and A-LMB during the uptake process are displayed in Fig. 2b. From Fig. 2a–b, it is observed that the capture kinetics of $H_iPO_4^{i-3}$ by R-LMB and A-LMB are characterized by a rapid adsorption in the early uptake stage and a slow adsorption during the gradual uptake period. The fast adsorption of $H_iPO_4^{i-3}$ onto R-LMB and A-LMB during the early capture period was mainly due to the fact that at the beginning of the uptake process, the active adsorption sites on the surfaces of R-LMB and A-LMB were abundant, and the difference in the initial $H_iPO_4^{i-3}$ concentration between the water and the surfaces of R-LMB and A-LMB was large (Zhang et al., 2022). To further investigate the relation between $H_iPO_4^{i-3}$ adsorption by R-LMB or A-LMB and contact time, three commonly used equations (QFO, QSO and Elovich equations) (Jiang et al., 2021; Khnifira et al., 2023; Tran et al., 2017) were used to fit the experimental kinetics data. The fitted parameters of QFO, QSO and Elovich equations are presented in Table 2. The results in Table 2 suggest that the Elovich equation ($R^2 = 0.971$ and 0.986 for R-LMB and A-LMB, respectively) can better reflect the $H_iPO_4^{i-3}$ adsorption kinetics of R-LMB and A-LMB than the QSO equation ($R^2 = 0.891$ and 0.921 for R-LMB and A-LMB, respectively). Furthermore, the QSO equation fits to the $H_iPO_4^{i-3}$ adsorption kinetics of R-LMB and A-LMB better than the QFO equation ($R^2 = 0.722$ and 0.764 for R-LMB and A-LMB, respectively). The Elovich equation has been widely used to describe chemisorptions data (Tran et al., 2017). The good fitting of the Elovich equation to the kinetic data in this study (Table 2) indicates that the adsorption of $H_iPO_4^{i-3}$ on R-LMB or A-LMB is chemisorption process. This conclusion was further supported by the relatively good fitting of the QSO equation to the kinetic data of $H_iPO_4^{i-3}$ by R-LMB and A-LMB (Adil and Kim, 2023; Yin et al., 2022b). Under the same contact time condition, the amount of $H_iPO_4^{i-3}$ adsorbed onto A-LMB was lower than that onto R-LMB (Fig. 1a), demonstrating that the $Na^+/Ca^{2+}/Cl^-/HCO_3^-/SO_4^{2-}$ co-treatment can decrease the $H_iPO_4^{i-3}$ adsorption capacity. Based on the parameters of

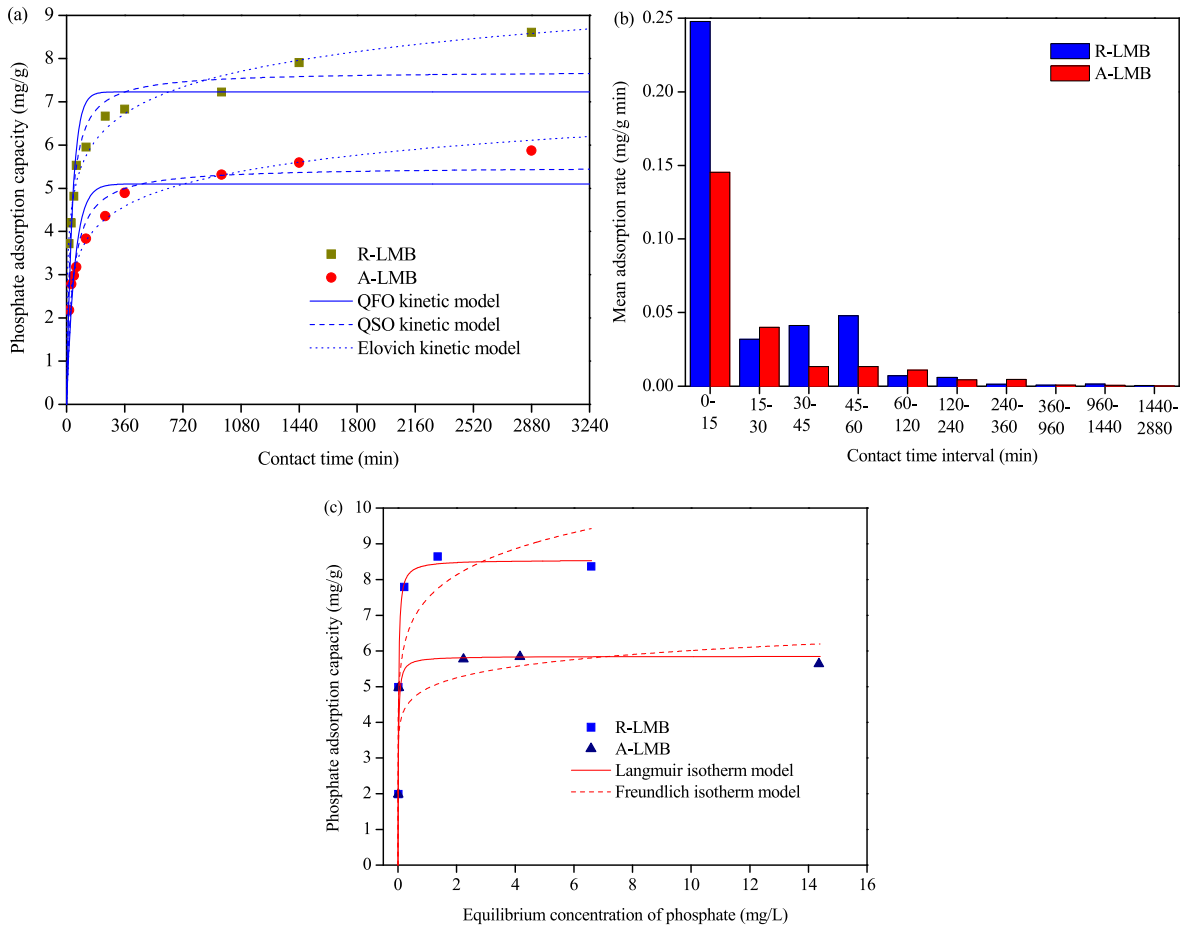

Fig. 2. Adsorption (a) kinetics and (c) isotherms of phosphate onto R-LMB and A-LMB; (b) average adsorption rate of phosphate onto R-LMB and A-LMB.

Table 2
QFO, QSO and Elovich kinetics parameters for phosphate adsorption onto R-LMB and A-LMB.

Kinetic models	Parameters	R-LMB	A-LMB
QFO kinetic model	q_e (mg/g)	7.23	5.10
	K_1 (1/min)	0.0281	0.0198
	R^2	0.722	0.764
QSO kinetic model	q_e (mg/g)	7.71	5.50
	K_2 (g/mg min)	0.00540	0.00499
	v_0 (mg/g min)	0.321	0.151
	R^2	0.891	0.921
Elovich kinetic model	α (mg/g min)	4.63	1.04
	β (g/mg)	1.12	1.36
	R^2	0.971	0.986

the QSO equation, the initial rates of $H_iPO_4^{i-3}$ onto R-LMB and A-LMB were calculated to be 0.321 and 0.151 mg/g min, respectively (Table 2). The initial $H_iPO_4^{i-3}$ adsorption rates of R-LMB and A-LMB derived from the Elovich kinetics model were 4.63 and 1.04 mg/g min, respectively (Table 2). The average $H_iPO_4^{i-3}$ adsorption rates of R-LMB and A-LMB during the period of 0–15 min were determined to be 0.248 and 0.145 mg/g min, respectively (Fig. 2b). Clearly, compared to A-LMB, phosphate can be more quickly removed by R-LMB in the initial adsorption stage. In other word, the combined aging treatment of R-LMB with Na^+, Ca^{2+}, Cl^-, HCO_3^- and SO_4^{2-} can reduce the rate of $H_iPO_4^{i-3}$ adsorption in the initial capture stage.

3.2.2. *Adsorption isotherms*

The isotherm data of $H_iPO_4^{i-3}$ adsorption onto R-LMB and A-LMB are presented in Fig. 2c. The experimental data of $H_iPO_4^{i-3}$ adsorption onto R-LMB and A-LMB were fitted using two commonly isotherm equations (Langmuir and Freundlich equations)(Freundlich, 1926; Langmuir, 1916), as shown in Fig. 2c. Table 3 summarizes the estimated parameters of Langmuir and Freundlich equations for $H_iPO_4^{i-3}$ adsorption onto R-LMB and A-LMB. It is observed from Fig. 2c that the $H_iPO_4^{i-3}$ adsorption capacities of R-LMB and A-LMB increased with the increase of P equilibrium concentration until the equilibrium adsorption came up to a saturation state. It can be seen from Fig. 2c and Table 3 that the Langmuir equation (R^2 = 0.877 and 0.741 for R-LMB and A-LMB, respectively) had the higher fitting degree with the adsorption isotherm data of $H_iPO_4^{i-3}$ by R-LMB and A-LMB than the Freundlich equation (R^2 = 0.586 and 0.442 for R-LMB and A-LMB, respectively). This indicates that the adsorption of $H_iPO_4^{i-3}$ onto R-LMB or A-LMB belongs to monolayer adsorption (Kim et al., 2023; Rezania et al., 2022). According to the Langmuir isotherm, the maximum capacities of adsorbed $H_iPO_4^{i-3}$ on R-LMB and A-LMB were calculated to be 8.55 and 5.85 mg/g, respectively. The greatest $H_iPO_4^{i-3}$ adsorption capacity for A-LMB was 31.6% less than that for R-LMB. This further demonstrates that the combined aging treatment of R-LMB with Na^+, Ca^{2+}, Cl^-, HCO_3^- and

Table 3
Langmuir and Freundlich isotherm parameters for phosphate adsorption onto R-LMB and A-LMB.

Isotherm model	Parameter	R-LMB	A-LMB
Langmuir isotherm model	q_s (mg/g)	8.55	5.85
	k_L (L/mg)	56.1	66.0
	R^2	0.877	0.741
Freundlich isotherm model	k_F	7.46	4.95
	$1/n$	0.124	0.0844
	R^2	0.586	0.442

SO_4^{2-} can inhibit the adsorption of $H_iPO_4^{i-3}$.

3.2.3. Effect of adsorbent dosage on adsorption

The possible impact of adsorbent dosage on the $H_iPO_4^{i-3}$ capture by R-LMB and A-LMB was explored in this study. Fig. 3a shows the corresponding findings. As illustrated in Fig. 3a, the $H_iPO_4^{i-3}$ removal efficiencies of R-LMB and A-LMB both increased with the increase of adsorbent dosage. This is because that the number of adsorbent active sites increases with the increase of adsorbent dosage (Moumen et al., 2022; Zhong et al., 2020). When the adsorbent dosage increased from 0.2 to 0.4 g/L and from 0.8 to 1.2 g/L, the $H_iPO_4^{i-3}$ adsorption capacities for R-LMB and A-LMB decreased. However, the $H_iPO_4^{i-3}$ adsorption capacities for R-LMB and A-LMB basically remained unchangeable with the increase in the adsorbent dosage from 0.4 to 0.8 g/L. This indicates high $H_iPO_4^{i-3}$ adsorption capacities for R-LMB and A-LMB at a low adsorbent dosage. This is due to the fact that when the adsorbent dosage is low, all active sites on the adsorbent surface are occupied, saturating the surface (Isidoro Ribeiro et al., 2023). Under the same adsorbent dosage condition, the $H_iPO_4^{i-3}$ removal efficiency of R-LMB was larger than that of A-LMB, and the former also had a higher $H_iPO_4^{i-3}$ adsorption capacity than the latter, further confirming the inhibition of $H_iPO_4^{i-3}$ adsorption onto LMB by the combined aging treatment with Na^+, Ca^{2+}, Cl^-, HCO_3^- and SO_4^{2-}.

3.2.4. Effect of solution pH on adsorption

The possible impact of pH on the $H_iPO_4^{i-3}$ capture by R-LMB and A-LMB was explored in this study. Fig. 3b shows the corresponding findings. As displayed in Fig. 3b, the $H_iPO_4^{i-3}$ uptake capacities of R-LMB and A-LMB decreased as the solution pH increased. The decrease in the $H_iPO_4^{i-3}$ adsorption performance for R-LMB with increasing solution pH has been observed in the previous studies (Haghseresht et al., 2009; Kang et al., 2022; Reitzel et al., 2013; Ross et al., 2008). Previous studies have shown that the major mechanism for the adsorption of $H_iPO_4^{i-3}$ onto lanthanum-based adsorbents in the form of lanthanum ion is precipitation and electrostatic attraction, while the major mechanism of lanthanum carbonate-based adsorbents is ligand exchange and electrostatic attraction (He et al., 2022). Dithmer et al. found that all $H_iPO_4^{i-3}$ was immobilized as rhabdophane ($LaPO_4{\cdot}nH_2O$, $n \leq 3$) after the uptake of $H_iPO_4^{i-3}$ by lanthanum exchanged bentonite (Dithmer et al., 2015). Therefore, we deduced that the formation of rhabdophane is an important mechanism that dominates the adsorption of $H_iPO_4^{i-3}$ onto R-LMB and A-LMB. In addition, since R-LMB and A-LMB contained lanthanum carbonate, the ligand exchange and inner-sphere La–P complex formation should play a role in the uptake of $H_iPO_4^{i-3}$ by R-LMB and A-LMB. The lanthanum ion has a greater affinity for $H_2PO_4^-$ than for HPO_4^{2-} (Haghseresht et al., 2009). When the solution pH increases from 5 to 10, the amount of HPO_4^{2-} increases but the amount of $H_2PO_4^-$ decreased (Liu et al., 2012). This results in the decrease in the precipitation of $H_iPO_4^{i-3}$ with La^{3+} and thus leads to the decrease of the $H_iPO_4^{i-3}$ adsorption capacities for R-LMB and A-LMB. In addition, the increase in the solution pH from 7 to 10 can give rise to the formation of the hydroxyl species of the lanthanum species and thus the decrease in the number of phosphate binding sites on the surfaces of lanthanum exchanged bentonite (Ross et al., 2008). This also can give rise to a delay in the generation of rhabdophane and thus the decreasing $H_iPO_4^{i-3}$ adsorption capacities for R-LMB and A-LMB with the increase of solution pH from 7 to 10. Under basic condition, competitive adsorption from hydroxyl ions can restrain the adsorption of $H_iPO_4^{i-3}$, and ligand exchange between $H_iPO_4^{i-3}$ and adsorbent is inhibited (Chen et al., 2020; Yang et al., 2021). The ligand exchange even stops when the solution pH is too high (Yang et al., 2021). Therefore, with the increase of solution pH, the ligand exchange between $H_iPO_4^{i-3}$ and lanthanum carbonate is

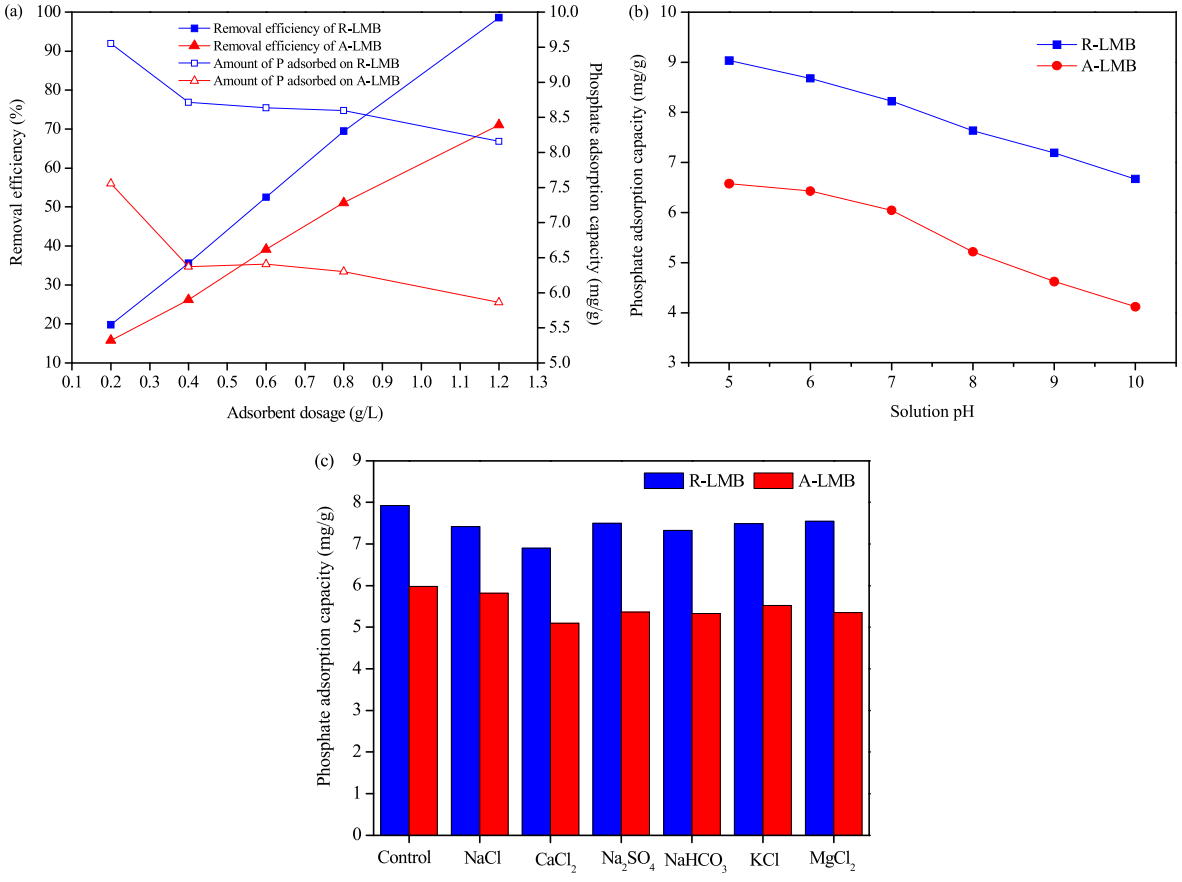

Fig. 3. Effects of (a) adsorbent dosage, (b) solution pH and (c) co-existing electrolyte on phosphate adsorption onto R-LMB and A-LMB.

weakened, also resulting in the decrease in the $H_iPO_4^{i-3}$ adsorption capacities for R-LMB and A-LMB. Furthermore, higher OH^- concentration induced by the increase in the solution pH caused the competition between OH^- and $H_iPO_4^{i-3}$ for the active adsorption sites of lanthanum carbonate (Koh et al., 2020), also thus resulting in the decreased $H_iPO_4^{i-3}$ adsorption capacities for R-LMB and A-LMB. Under the same pH condition, the amount of $H_iPO_4^{i-3}$ adsorbed by R-LMB was larger than that by A-LMB, further confirming the inhibition of $H_iPO_4^{i-3}$ adsorption onto LMB by the combined aging treatment with Na^+, Ca^{2+}, Cl^-, HCO_3^- and SO_4^{2-}.

3.2.5. *Effect of coexisting anions and cations on adsorption*

Fig. 3c shows the influences of coexisting Na^+, Ca^{2+}, K^+, Mg^{2+}, Cl^-, HCO_3^- and SO_4^{2-} on the $H_iPO_4^{i-3}$ capture by R-LMB and A-LMB. The $H_iPO_4^{i-3}$ adsorption capacities for R-LMB in the presence of NaCl, $CaCl_2$, KCl, $MgCl_2$, Na_2SO_4 and $NaHCO_3$ were 6.30%, 12.8%, 5.42%, 4.79%, 5.29% and 7.56% less than that in the absence of any coexisting electrolyte. This indicates that coexisting Na^+, Ca^{2+}, K^+, Mg^{2+}, Cl^-, SO_4^{2-} and HCO_3^- all can hinder the $H_iPO_4^{i-3}$ capture by R-LMB. The amounts of $H_iPO_4^{i-3}$ adsorbed onto A-LMB with coexisting NaCl, $CaCl_2$, KCl, $MgCl_2$, Na_2SO_4 and $NaHCO_3$ were 2.83%, 14.8%, 7.67%, 10.7%, 10.3% and

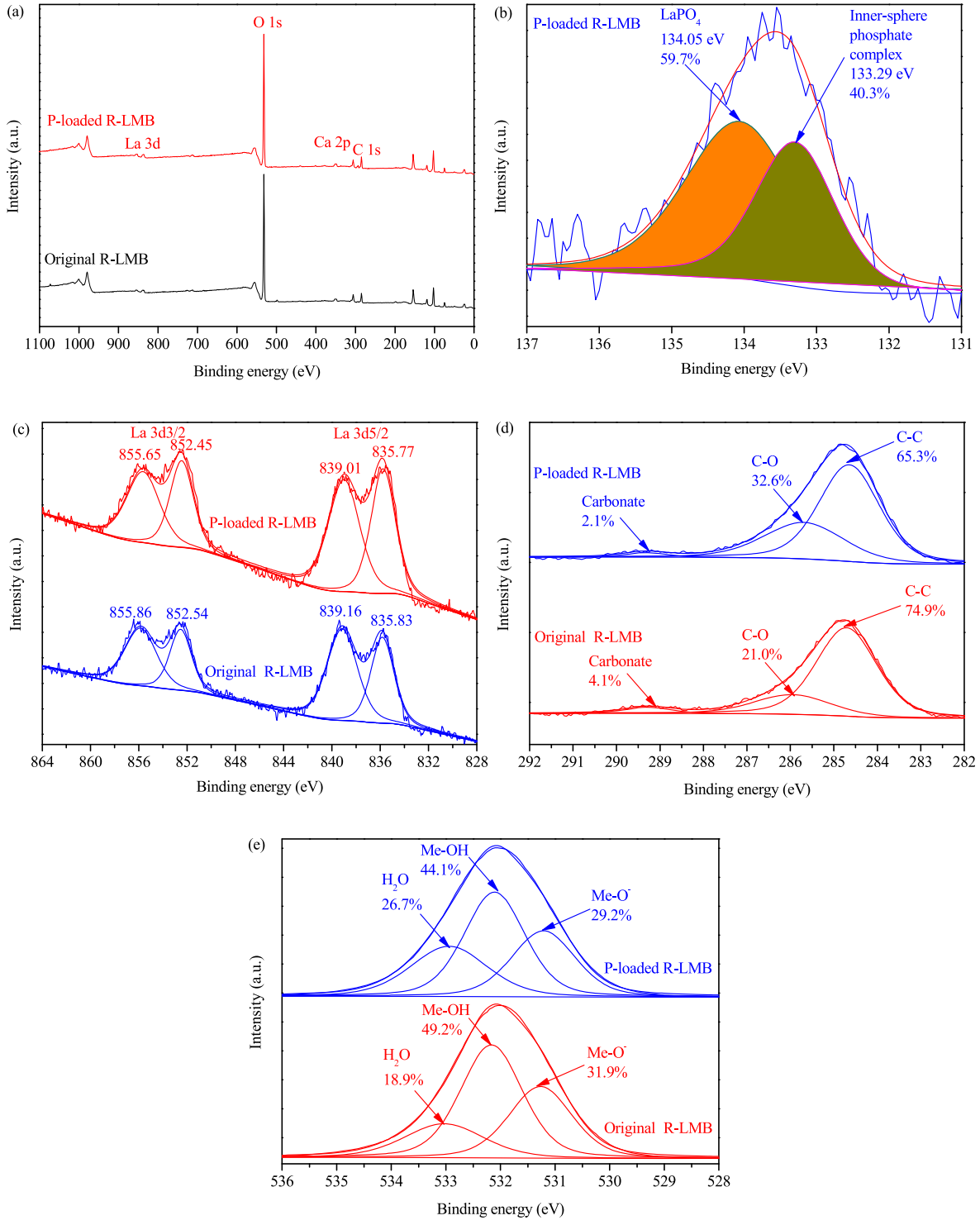

Fig. 4. XPS spectra of original and phosphate-adsorbed R-LMB samples. (a) Wide scan; (b) P 2p; (c) La 3d; (d) C 1s; (e) O 1s.

11.0% less than that without any coexisting electrolyte. This means that coexisting Na^+, Ca^{2+}, K^+, Mg^{2+}, Cl^-, HCO_3^- and SO_4^{2-} all can suppress the adsorption of $H_iPO_4^{i-3}$ onto A-LMB. Reitzel et al. found that when LMB was added to the water, the LMB dispersed (Reitzel et al., 2013). The dispersion of LMB in water was higher in low alkalinity than that in high alkalinity water, giving rise to the improvement of SRP adsorption onto the LMB in the low alkalinity water (Reitzel et al., 2013). Furthermore, the lower concentration of Ca^{2+} in water can create a more pronounced dispersion of LMB and an improved surface area to volume ratio, thus resulting in the enhanced SRP adsorption by the LMB (Reitzel et al., 2013). Another previous study found that after the addition of LMB into water, the concentration of filtered lanthanum in the soft water was higher compared to the hard water (Reitzel et al., 2017). Thus, we deduced that the presence of Ca^{2+} inhibited the dispersion of LMB and the release of lanthanum ion from LMB, which resulted in the decreased $H_iPO_4^{i-3}$ adsorption capacities for R-LMB and A-LMB. In the presence of NaCl, $CaCl_2$, KCl, $MgCl_2$, Na_2SO_4 or $NaHCO_3$, the amount of $H_iPO_4^{i-3}$ adsorbed onto R-LMB was higher than that onto A-LMB, which further confirms that the uptake of $H_iPO_4^{i-3}$ by LMB is hindered by the combined aging treatment with Na^+, Ca^{2+}, Cl^-, HCO_3^- and SO_4^{2-}.

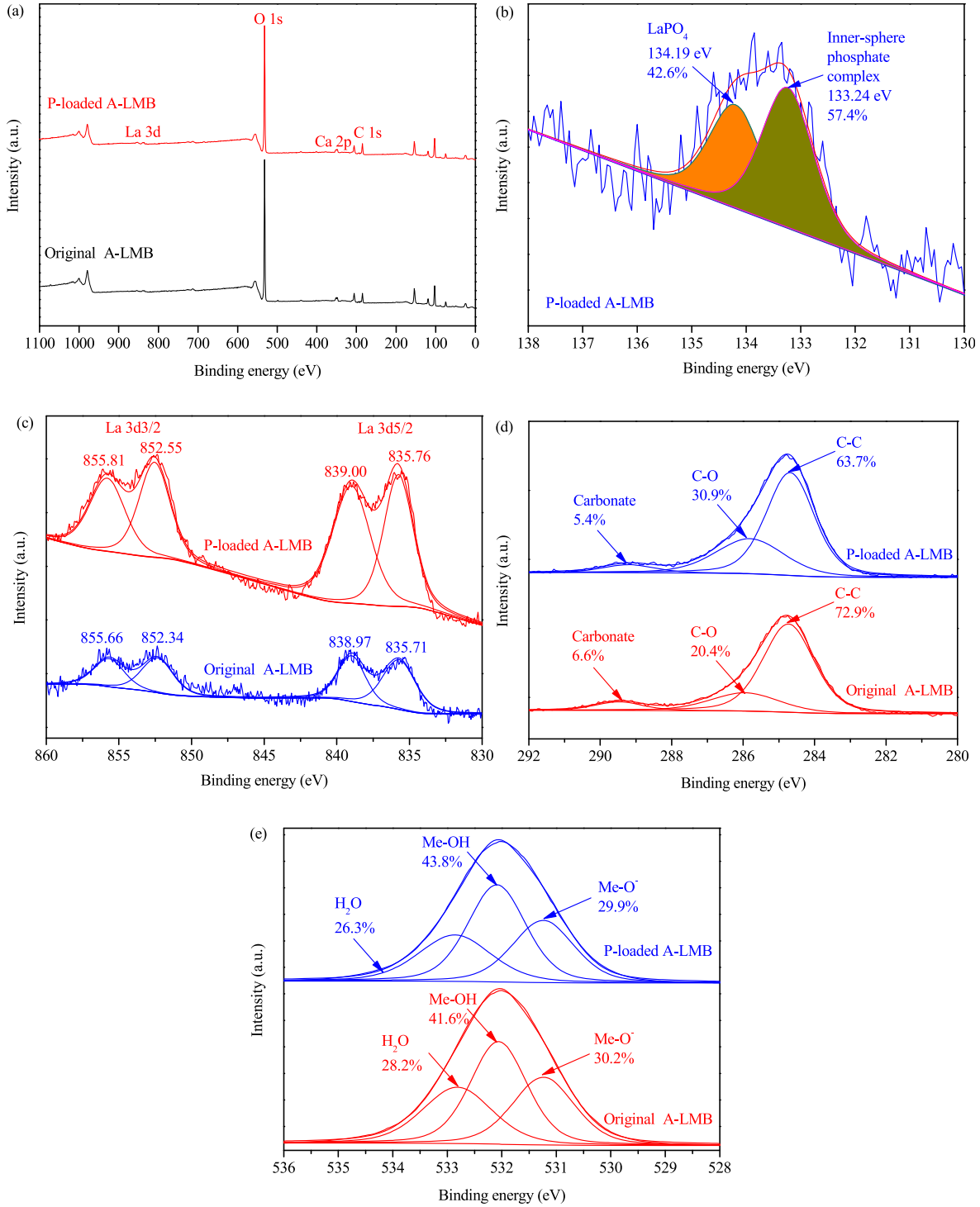

Fig. 5. XPS spectra of original and phosphate-adsorbed A-LMB samples. (a) Wide scan; (b) P 2p; (c) La 3d; (d) C 1s; (e) O 1s.

3.2.6. Adsorption mechanisms

In order to explore the influence of the combined aging treatment with Na^+, Ca^{2+}, Cl^-, HCO_3^- and SO_4^{2-} on the mechanism for the $H_iPO_4^{i-3}$ capture by LMB, the XPS technique was used to characterize the R-LMB and A-LMB samples prior to and after the uptake of $H_iPO_4^{i-3}$.

The XPS spectra of R-LMB samples prior to and after $H_iPO_4^{i-3}$ uptake are displayed in Fig. 4. The existence of oxygen, lanthanum and calcium was confirmed by the wide-scan XPS spectra of the original and $H_iPO_4^{i-3}$-loaded R-LMB (Fig. 4a). The binding energy (BE) of P 2p peak for the $H_iPO_4^{i-3}$-loaded LMB was 133.55 eV (Fig. 3b), confirming that LMB successfully adsorbs $H_iPO_4^{i-3}$ after the contact of LMB with $H_iPO_4^{i-3}$ solution. The P 2p peak was separated into two peaks corresponding to $LaPO_4$ (134.05 eV) and inner-sphere lanthanum-phosphate complex (133.29 eV), and the corresponding relative areas were 59.7% and 40.3%, respectively (Fig. 4b). This suggests that the uptake of $H_iPO_4^{i-3}$ by R-LMB involves multiple reactions, and the precipitation of phosphate with lanthanum ion and the formation of inner-sphere lanthanum-phosphate complex played a key role in the $H_iPO_4^{i-3}$ capture by R-LMB. After the $H_iPO_4^{i-3}$ capture by R-LMB, the characteristic peaks of La 3d5/2 shifted from 835.83 eV to 835.77 and from 839.16 eV to 839.01 eV, and those of La 3d3/2 shifted from 852.54 eV to 852.45 eV and from 855.86 eV to 855.65 eV (Fig. 4c). This also indicates the formation of $LaPO_4$ and inner-sphere La–O–P complexes after the uptake of $H_iPO_4^{i-3}$ by R-LMB. After the adsorption of $H_iPO_4^{i-3}$ onto R-LMB, the relative area of carbonate to total carbon decreased (Fig. 4d), confirming that the ligand exchange occurs between the $H_iPO_4^{i-3}$ in water and the carbonate group of lanthanum carbonate in LMB during the adsorption process (Liang et al., 2023). The O 1s spectrum of the original R-LMB (Fig. 4e) included three overlapped peaks, which are ascribed to metal oxide oxygen (Me–O^-), hydroxyl group oxygen (Me–OH) and adsorbed water molecule (H_2O), respectively (Yang et al., 2022b). After the adsorption of $H_iPO_4^{i-3}$ onto R-LMB, the relative area of Me–OH to total oxygen decreased from 49.2% to 44.1%. This indicates that hydroxyl group participates in the adsorption process of $H_iPO_4^{i-3}$ onto R-LMB, and the ligand exchange between hydroxyl group and $H_iPO_4^{i-3}$ should have a role in the $H_iPO_4^{i-3}$ capture by R-LMB. In summary, the precipitation of $H_iPO_4^{i-3}$ with La^{3+} to form $LaPO_4$ and the ligand exchange between carbonate/hydroxyl groups and $H_iPO_4^{i-3}$ to form the inner-sphere lanthanum-phosphate complexes are key mechanisms for the uptake of $H_iPO_4^{i-3}$ by R-LMB at pH 7.

The XPS spectra of A-LMB samples prior to and after $H_iPO_4^{i-3}$ uptake are shown in Fig. 5. The existence of oxygen, lanthanum and calcium was confirmed by the full-scan XPS spectra of the fresh and $H_iPO_4^{i-3}$-adsorbed A-LMB samples (Fig. 5a). As illustrated in Fig. 5b, the BE of P 2p peak for the $H_iPO_4^{i-3}$-adsorbed A-LMB was 133.85 eV, demonstrating the successful capture of $H_iPO_4^{i-3}$ onto A-LMB. The P 2p peaks in the P-loaded A-LMB can be separated into two peaks ascribed to $LaPO_4$ and inner-sphere lanthanum-phosphate complexes, and the corresponding percentages were 42.6% and 57.4%, respectively (Fig. 5b). This indicates that the major mechanisms that govern the $H_iPO_4^{i-3}$ capture by A-LMB include the generation of $LaPO_4$ and inner-sphere lanthanum-phosphate complexes. After the $H_iPO_4^{i-3}$ uptake by A-LMB, the characteristic peaks of La 3d5/2 shifted from 835.71 eV to 835.76 eV and from 838.97 eV to 839.00 eV, and those of La 3d3/2 shifted from 852.34 eV to 852.55 eV and from 855.66 eV to 855.81 eV (Fig. 5c), further confirming the $LaPO_4$ and inner-sphere lanthanum-phosphate complexes formation. The relative area of carbonate to total carbon for the fresh A-LMB was larger than that for the P-loaded A-LMB (Fig. 5d), demonstrating the ligand exchange between CO_3^{2-} and $H_iPO_4^{i-3}$ after the capture of $H_iPO_4^{i-3}$ by A-LMB. After the uptake of $H_iPO_4^{i-3}$ by A-LMB, the relative area of Me–OH to total oxygen increased. This indicates that the ligand exchange between hydroxyl group and $H_iPO_4^{i-3}$ is not the mechanism that dominates the adsorption of $H_iPO_4^{i-3}$ on A-LMB. Based on all the results in Fig. 5, we conclude that the precipitation of $H_iPO_4^{i-3}$ with La^{3+} to form $LaPO_4$ and the ligand exchange between carbonate group and $H_iPO_4^{i-3}$ to form the inner-sphere lanthanum-phosphate complexes are key mechanisms for the uptake of $H_iPO_4^{i-3}$ by A-LMB at pH 7.

Based on all the experimental results in Figs. 4 and 5, it can be concluded that the combined aging treatment with Na^+, Ca^{2+}, Cl^-, HCO_3^- and SO_4^{2-} can only have a limited effect on the mechanism for the uptake of $H_iPO_4^{i-3}$ by LMB, and the precipitation of phosphate with lanthanum ion to form $LaPO_4$ and the ligand exchange between CO_3^{2-} and $H_iPO_4^{i-3}$ to form the inner-sphere lanthanum-phosphate complexes are still the important mechanisms for the $H_iPO_4^{i-3}$ uptake by LMB after the combined aging treatment with Na^+, Ca^{2+}, Cl^-, HCO_3^- and SO_4^{2-}.

The negative effect of the combined aging treatment with Na^+, Ca^{2+}, Cl^-, HCO_3^- and SO_4^{2-} on the adsorption of $H_iPO_4^{i-3}$ on LMB can be explained as follows. The content of Ca^{2+} in R-LMB was lower than that in A-LMB (Table 1). Lower Ca^{2+} loading in LMB will lead to thicker double layers and a larger repulsion of charged particles, which will result in a larger degree of LMB particle dispersion and thus a higher risk of lanthanum ion release (Reitzel et al., 2013, 2017). Higher Ca^{2+} loading in LMB will result in thinner double layers and a small repulsion of charged particles, which will give rise to low LMB particle dispersion and consequently low lanthanum ion concentration (Reitzel et al., 2013, 2017). The aggregation and low La dissolution are unfavorable for the removal of $H_iPO_4^{i-3}$ by LMB, while the dispersion and high La dissolution are favorable for the removal of $H_iPO_4^{i-3}$ by LMB (Reitzel et al., 2017), resulting in that the LMB with higher Ca^{2+} loading (i.e., A-LMB) has a lower $H_iPO_4^{i-3}$ adsorption capacity than the LMB with lower Ca^{2+} loading (i.e., R-LMB).

3.3. Effect of R-LMB and A-LMB on P mobilization in sediment

3.3.1. Effect of R-LMB and A-LMB on SRP and DTP of overlying water

The changes of pH, SRP and DTP in OW with the incubation time are presented in Fig. 6. The elimination rates of SRP and DTP from OW by the R-LMB and A-LMB treatments (addition and capping) are also presented in Fig. 6. As illustrated in Fig. 6a, the pH values of OW for the control, R-LMB addition, A-LMB addition, R-LMB capping and A-LMB capping columns varied from 7.24 to 7.52, 7.10 to 7.51, 7.13 to 7.57, 7.23 to 7.49, and 7.09 to 7.46, respectively. This indicates that the overlying water in the control group was maintained in near neutral state, and the R-LMB and A-LMB treatments (addition and capping) had a limited impact on the pH value in the overlying water. With the increase of incubation time from 0 to 56 and 67–244 days, the concentration of SRP in OW increased (Fig. 6b). Although the concentration of SRP in OW decreased as the incubation time increased from 56 to 67 and from 244 to 282 days, the concentrations of SRP in OW on the 67th and 282nd days were obviously higher than that at the initial time. When the experimental time rose from 0 to 244 days, the concentration of DTP in OW increased (Fig. 6d). Although the increase in the experimental time from 244 to 282 days brought about the decrease in the DTP concentration of OW, the concentration of DTP in OW on day 282 was significantly higher than that at the initial time (Fig. 6d). These results demonstrate that the liberation of phosphorus from sediment under hypoxia condition takes place. The SRP concentrations of OW in the R-LMB addition, A-LMB addition, R-LMB covering and A-LMB covering groups during the anoxic period were 0.012–0.078, 0.016–0.093, 0.009–0.064 and 0.022–0.069 mg/L, respectively, which were remarkably lower than that of the control group (0.079–0.696 mg/L)(Fig. 6b). After the R-LMB addition, A-LMB addition, R-LMB covering and A-LMB covering, the SRP concentrations of OW decreased by 84.9%–94.4%, 78.6%–89.9%, 84.8%–95.7% and 67.7%–90.1%, respectively (Fig. 6c). Similarly, the R-LMB addition, A-LMB addition, R-LMB covering and A-LMB covering also led to the decrease in the concentration of DTP in OW during anoxia period (Fig. 6d–e). These results mean that the effectiveness of R-LMB and A-LMB in the restraint of phosphorus liberation from sediment into OW under hypoxia condition is excellent. The elimination rate of OW SRP by the R-LMB addition was larger than that by the A-LMB addition (Fig. 6c), and the reduction efficiency of OW DTP by the former was also larger than that by the latter (Fig. 6e). This

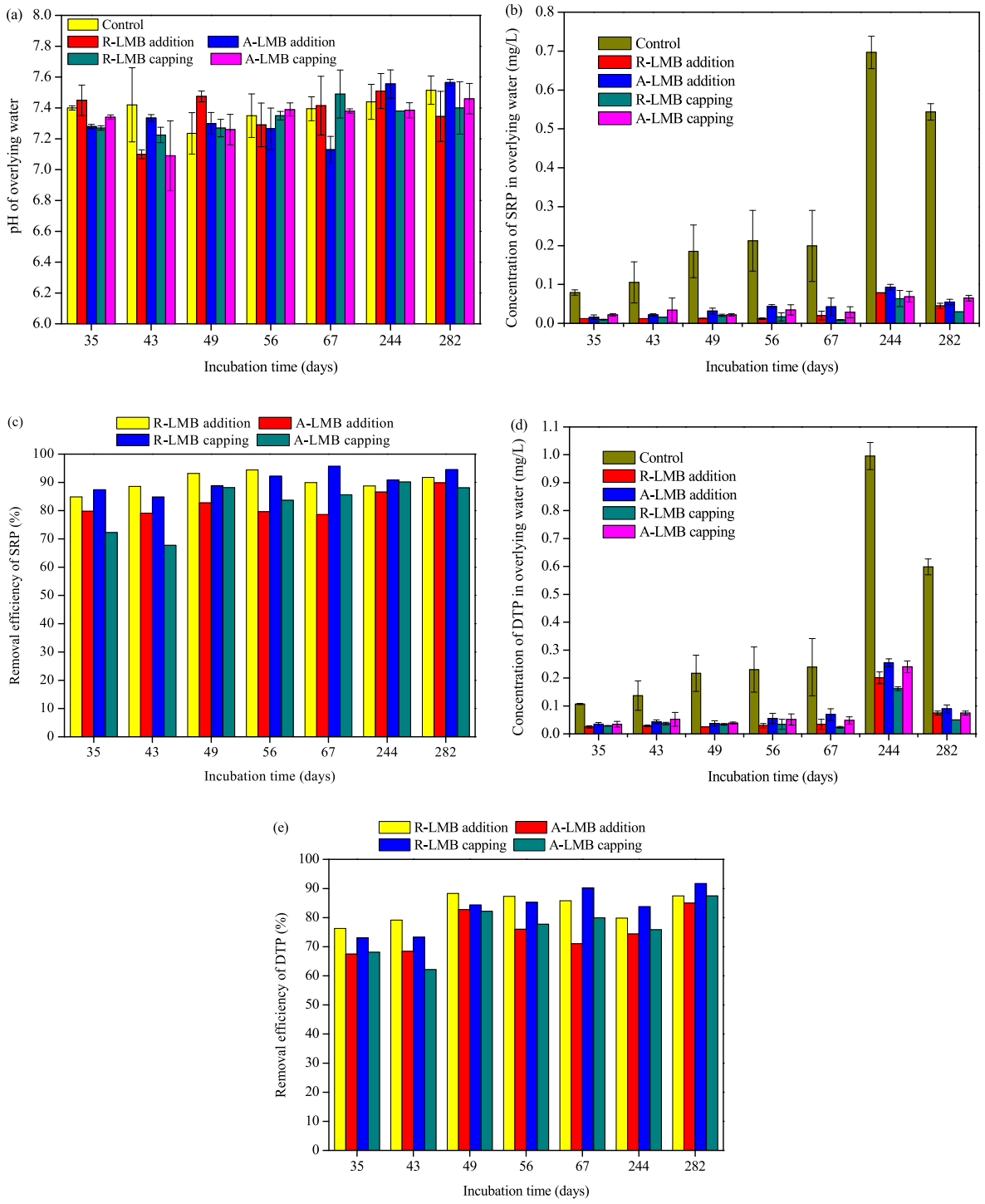

Fig. 6. Variations of (a) pH, (b) SRP and (d) DTP in OW for control, R-LMB addition, A-LMB addition, R-LMB capping and A-LMB capping groups; elimination rates of (c) SRP and (e) DTP in OW by R-LMB addition, A-LMB addition, R-LMB capping and A-LMB capping.

implies the lower efficiency of the A-LMB addition to limit the internal phosphorus release to OW during hypoxia period compared to the R-LMB addition. From Fig. 6c–e, it can also be observed that the A-LMB capping has a lower interception efficiency of internal phosphorus release to OW under anoxia condition than the R-LMB capping. The average reduction rates of SRP and DTP in OW by the R-LMB addition were calculated to 90.2% and 83.4%, respectively, and those by the A-LMB addition were calculated to be 82.3% and 75.0%, respectively. The mean eliminate rates of SRP and DTP by the R-LMB capping were computed to be 90.6% and 83.1%, respectively, and those by the A-LMB capping were computed to be 82.2% and 76.2%, respectively. Therefore, the combined aging treatment of LMB with Na^+, Ca^{2+}, Cl^-, HCO_3^- and SO_4^{2-} reduces the performance of LMB to restrain the liberation of endogenous phosphorus into OW under hypoxia conditions to a certain degree.

3.3.2. *Effect of R-LMB and A-LMB on DGT-unstable P and Fe of overlying water and sediment*

In order to further explore the effectiveness of R-LMB and A-LMB treatments (addition and capping) to hinder the internal phosphorus

release to OW and to illustrate the controlling mechanisms of R-LMB and A-LMB, the impacts of R-LMB and A-LMB treatments (addition and capping) on the distributions of DGT-UP and DGT-UF in the OW/sediment profile were studied. Fig. 7 shows the corresponding findings. From Fig. 7a–c, it is observed that the DGT-UP concentration gradient in the sediment and OW near the OW-sediment interface was obvious, indicating that the internal phosphorus can be released to the interstitial water (IW) and the dissolved P can be further transported to the overlying water under anoxia conditions. For the control group, the concentrations of DGT-UF in OW and sediment were 3.54–5.55 and 3.02–5.80 mg/L, respectively (Fig. 7e). This indicates that under hypoxia conditions, phosphorus can be leached from sediment through the reduction and dissolution of Fe(III) oxyhydroxides (Chen et al., 2016, 2018, 2019). The simultaneous release of phosphorus and iron from sediment under anoxia condition via the reduction and dissolution of Fe (III) minerals has been reported in previous literatures. After the R-LMB and A-LMB addition, the concentrations of DGT-UP in OW and sediment greatly decreased (Fig. 7a). The elimination rates of DGT-UP in OW and

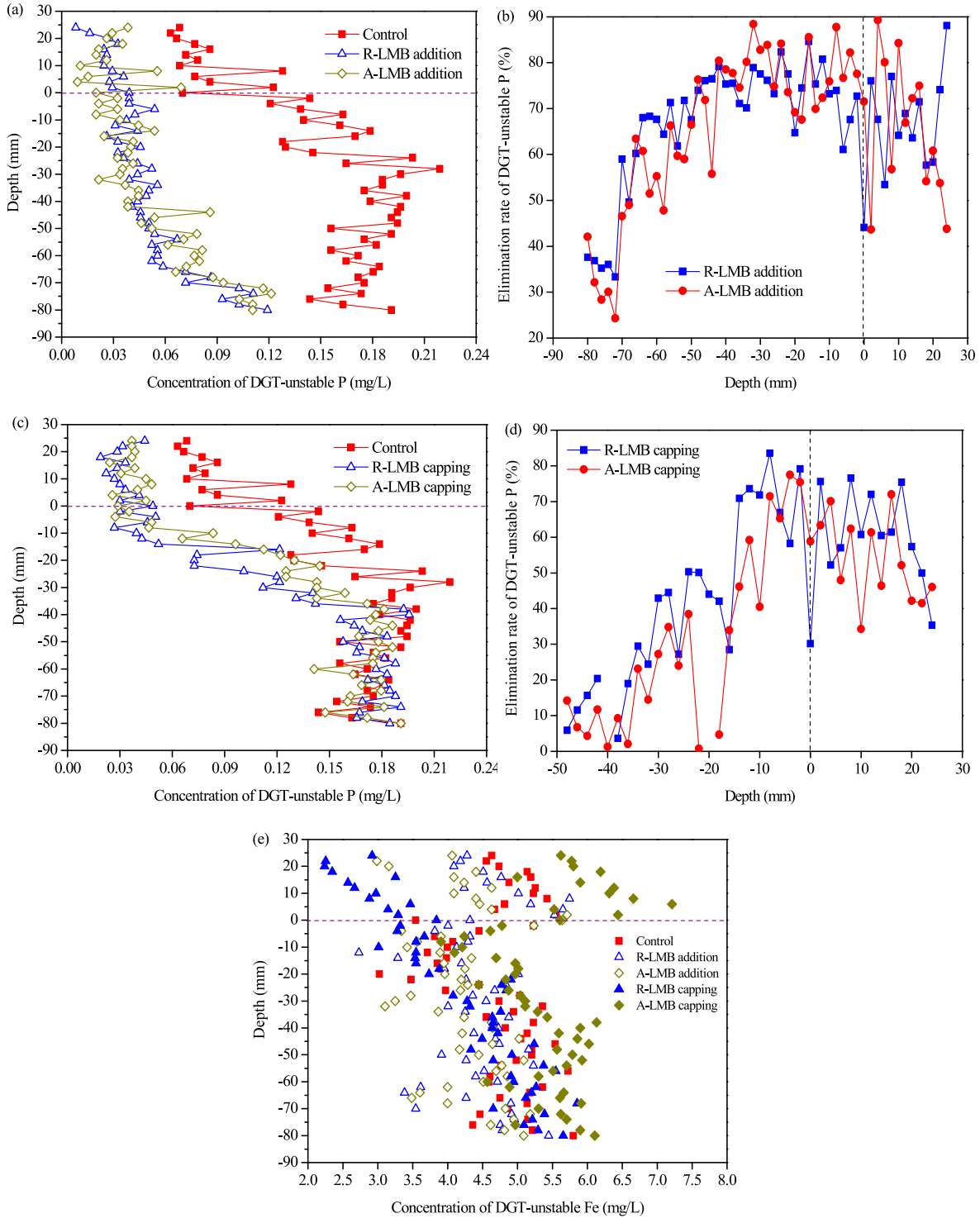

Fig. 7. Effect of LMB (a) addition and (c) capping on the concentrations of DGT-unstable P in the OW/sediment profile; elimination rates of DGT-unstable P by the LMB (b) addition and (d) capping; (e) concentrations of DGT-unstable Fe in the profile of OW and sediment for the control, LMB addition and LMB capping groups.

sediment by the R-LMB addition were 44.1%–88.1% and 33.3%–84.6%, respectively, and those by the A-LMB addition were 43.6%–89.3% and 24.3%–88.4%, respectively (Fig. 7b). After the R-LMB and A-LMB capping, the concentrations of DGT-UP in OW significantly decreased, and those in the upper sediment also significantly decreased (Fig. 7c). The elimination rates of DGT-UP in OW by the R-LMB and A-LMB capping were 30.2%–76.6% and 34.3%–72.0%, respectively, and the elimination rates of DGT-UP in the sediments at the depths of between −2 and −14 mm (minus signal indicates the location below the OW-sediment interface) by the R-LMB and A-LMB capping were 58.2%–83.5% and 40.5%–77.4%, respectively (Fig. 7d). These results demonstrate that under hypoxia conditions, the uses of R-LMB and A-LMB as capping and addition materials all can be effective in the restraint of internal phosphorus liberation to OW. In addition, the R-LMB and A-LMB addition both can be effective in the inactivation of DGT-UP in sediment, and the R-LMB and A-LMB capping both can effectively inactivate the DGT-UP in the top sediment layer. The effect of R-LMB and A-LMB addition on the distributions of DGT-UP in OW and sediment can be explained as follows. The presence of DGT-UF in the sediments for the R-LMB and A-LMB addition groups (Fig. 7e) indicate that under the action of R-LMB or A-LMB addition, P still can be leached from sediment to IW. However, the R-LMB or A-LMB located in sediment will adsorb the soluble phosphorus in IW, which will give rise to the decrease of soluble phosphorus concentration in the IW. Once the concentration of soluble P in IW decreases, the DGT-unstable P will be released to compensate the decrease of soluble phosphorus concentration in the IW. The capture rate of P in IW by R-LMB or A-LMB is expected to be significantly larger than the release rate of P from sediment to IW, resulting in the obvious decrease of DGT-unstable P in sediment under the condition of R-LMB or A-LMB addition. This further induces the reduction in the flux of phosphorus diffusion from IW to OW (Norgbey et al., 2020), thus reducing the concentration of DGT-UP in the overlying water. Since the DGT-unstable P in sediment has a high releasing risk, the formation of phosphorus static layer (P-SL) in sediment caused by the inactivation of DGT-UP is very important for the restraint of internal phosphorus release to OW. The influence of R-LMB and A-LMB capping on the distributions of DGT-UP in OW and sediment can be explained as follows. Under the action of R-LMB or A-LMB covering, P still can leached from sediment to IW via the reductive dissolution of Fe (III)-bound P. The R-LMB or A-LMB capping can adsorb the soluble P in the sediment near the capping layer. After the soluble phosphorus concentration in the sediment near the capping layer decreases, the DGT-unstable phosphorus in sediment will be liberated to make up the decrease of soluble phosphorus concentration. The releasing rate of DGT-UP should be substantially lower than the rate of P capture by the R-LMB or A-LMB covering layer, which will give rise to the obvious decrease of DGT-UP concentration in the top sediment. The lower concentration of DGT-UP in the top sediment will cause the lower flux of phosphorus diffusion from IW to OW (Norgbey et al., 2020), finally leading to the lower concentration of DGT-UP in OW under R-LMB or A-LMB capping condition. Wang et al. found that the formation of P-SL is vital to the control of endogenous phosphorus release to OW by the LMB capping (Wang et al., 2017). Consequently, the formation of P-SL in the top sediment induced by the inactivation of DGT-UP is very important for the interception of internal phosphorus liberation to OW by the R-LMB and A-LMB capping.

It is worth noting that the mean concentrations of DGT-UP in OW for the R-LMB and A-LMB capping groups were calculated to be 0.032 and 0.037 mg/L, respectively. The mean elimination rates of DGT-UP in OW by the R-LMB and A-LMB capping were calculated to be 58.8% and 53.7%, respectively. It is obvious that the mean concentration of DGT-UP in OW under R-LMB capping condition was less than that under A-LMB capping condition, and the R-LMB capping had a higher elimination rate of DGT-UP from OW than the A-LMB capping. This further confirms that the A-LMB capping has a lower controlling efficiency of endogenous phosphorus release into OW under anoxia conditions that the R-LMB capping. The average concentrations of DGT-UP in the sediments at the depths of between −2 and −36 mm for the R-LMB and A-LMB capping groups were computed to be 0.083 and 0.107 mg/L, respectively, and the mean elimination rates of DGT-UP in the sediments at the depths of between −2 and −36 mm by the R-LMB and A-LMB capping were computed to be 50.4% and 37.6%, respectively. Obviously, the average DGT-UP concentration in the top 36 mm sediment under R-LMB capping condition was less than that under A-LMB capping condition, and the R-LMB capping had a higher elimination rate of DGT-UP in the top 36 mm sediment than the A-LMB capping, indicating that the A-LMB capping has a lower immobilization ability of DGT-UP in the upper sediment than the R-LMB capping. Therefore, the combined aging treatment of LMB with Na^+, Ca^{2+}, Cl^-, HCO_3^- and SO_4^{2-} is not conducive to the restraint of internal phosphorus release to OW by the LMB capping from the point of view of the sediment DGT-UP inactivation.

3.3.3. Effect of R-LMB and A-LMB on contents of potentially mobile P in sediment

Fig. 8 shows the LB-P, Fe–P and PM-P contents in sediments for the control, R-LMB addition, A-LMB addition, R-LMB capping and A-LMB capping groups. The sediments from the control, R-LMB addition, A-LMB addition, R-LMB capping and A-LMB capping groups contained a small amount of LB-P (Fig. 8a). After the R-LMB and A-LMB addition, the contents of Fe–P and PM-P in sediment obviously decreased (Fig. 8b–c). The reduction efficiencies of PM-P in the 0–10, 10–20, 20–30 and 30–50 mm sediment layers by the R-LMB addition were calculated to be 38.5%, 46.9%, 52.1% and 49.2%, respectively, and those by the A-LMB addition were calculated to be 38.1%, 41.4%, 41.6% and 35.4%, respectively. These results indicate that the R-LMB and A-LMB addition both can effectively inactivate the PM-P in sediment mainly via the immobilization of Fe–P. To be similar to the R-LMB or A-LMB addition, the R-LMB or A-LMB capping also can reduce the content of Fe–P in the 0–10 mm sediment layer (Fig. 8b). However, to be different to the R-LMB or A-LMB addition, the A-LMB or A-LMB capping had a limited influence on the content of Fe–P in the 10–100 mm sediment layer (Fig. 8b). The effect of R-LMB or A-LMB capping on the content of PM-P in sediment was similar to that on the quantity of Fe–P (Fig. 8b–c). Thus, the R-LMB and A-LMB capping both can immobilize the PM-P in the topmost sediment via the inactivation of Fe–P. PM-P can be liberated to IW and OW, thus making it a source of phosphorus for algal growth (Rydin, 2000; Tammeorg et al., 2022; Yang et al., 2023; Yin et al., 2022a). PM-P can reflect the internal P pollution level of sediment (Yang et al., 2023). Thus, the inactivation of PM-P in sediment acted as a significant role in the interception of internal phosphorus release to OW by the R-LMB and A-LMB addition, and the immobilization of PM-P in the topmost sediment acted as a significant role in the restraint of endogenous phosphorus liberation to OW by the R-LMB and A-LMB capping. The average elimination rates of PM-P in sediment by the R-LMB and A-LMB addition were calculated to be 46.7% and 39.1%, respectively. The reduction rates of PM-P in the 0–10 mm sediment layer by the R-LMB and A-LMB capping were computed to be 34.9% and 21.1%, respectively. This demonstrates that the R-LMB addition has a stronger immobilization ability of PM-P in sediment than the A-LMB addition, and the R-LMB capping exhibits a better inactivation performance of PM-P in the topmost sediment than the A-LMB capping. Consequently, the combined aging treatment of LMB with Na^+, Ca^{2+}, Cl^-, HCO_3^- and SO_4^{2-} is unfavorable for the interception of endogenous phosphorus liberation to OW by LMB from the point of view of the sediment PM-P inactivation.

3.3.4. Stability of P bound by R-LMB and A-LMB

Evaluating the stability of P adsorbed to the R-LMB and A-LMB capping layers is vital to understanding the mechanism of internal P release to OW by the LMB capping. Fig. 9 shows the speciation of P in the R-LMB and A-LMB capping layers. The contents of LB-P, Fe–P, NaOH-SRP, Ca–P and Res-P in the R-LMB capping layer were 1.50, 17.3, 18.9, 1.09×10^3 and 54.5 mg/kg, respectively (Fig. 8), which accounted

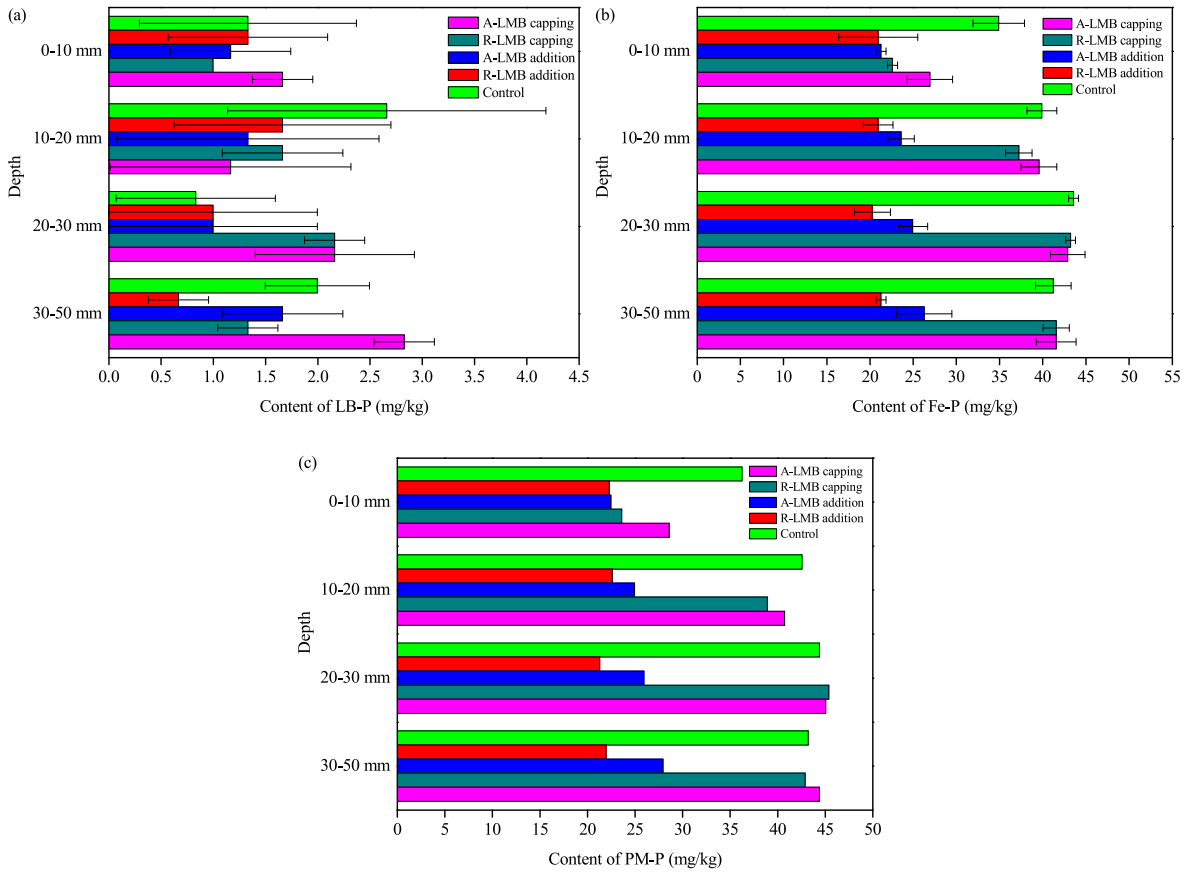

Fig. 8. Contents of (a) LB-P, (b) Fe–P and (c) PM-P in sediments for the control, LMB addition and LMB capping groups.

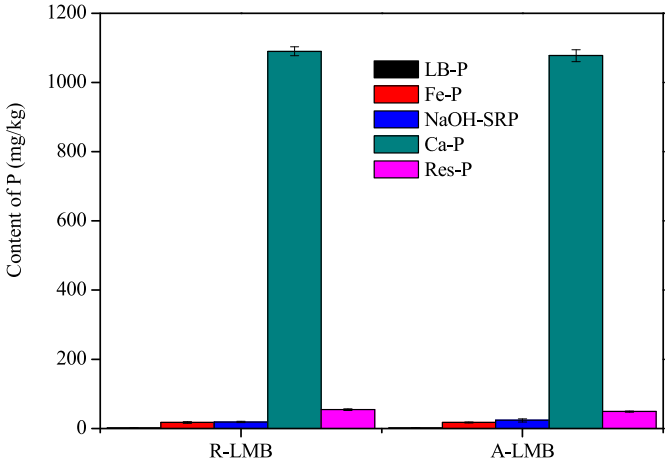

Fig. 9. P forms of R-LMB and A-LMB after their application to control P release from sediment.

for 0.127%, 1.46%, 1.60%, 92.2% and 4.61% of TP, respectively. The A-LMB capping layer had 1.66 mg/kg of LB-P, 17.6 mg/kg of Fe–P, 23.6 mg/kg of NaOH-SRP, 1.08 × 10^3 mg/kg of Ca–P and 48.9 mg/kg of Res-P (Fig. 9). The proportions of LB-P, Fe–P, NaOH-SRP, Ca–P and Res-P to TP in the A-LMB capping layer were computed to be 0.142%, 1.51%, 2.02%, 92.2% and 4.18%, respectively. The percentages of PM-P to TP in the R-LMB and A-LMB capping layers were calculated to be 1.59% and 1.65%, respectively. The proportion of relatively and very stable P (NaOH-SRP + Ca–P + Res-P) (Meis et al., 2012; Wang et al., 2013) to TP in the R-LMB or A-LMB capping layer was computed to be about 98.4%. This means that once the P that is released from sediment is adsorbed by the R-LMB and A-LMB capping layers, the overwhelming majority of immobilized P is difficult to be released into OW under common pH (5–9) and anoxia condition. The high stability of P immobilized by the R-LMB and A-LMB capping layers is conductive to the formation of P-SL in the upper sediment under the action of R-LMB and A-LMB capping.

3.4. Implication for application of LMB to control internal P release

This study indicates that the R-LMB capping can be effective in the interception of internal phosphorus liberation to OW under hypoxia condition. The inactivation of DGT-UP and PM-P in the topmost sediment acted as a key role in the restraint of endogenous P release to OW by the R-LMB capping. As we all know, Na^+, Ca^{2+}, Cl^-, HCO_3^- and SO_4^{2-} extensively existed in natural freshwater (DeVilbiss et al., 2022; Flower et al., 2022). After the application of R-LMB as a capping material to control the internal phosphorus pollution in freshwater bodies, the combined aging of R-LMB with Na^+, Ca^{2+}, Cl^-, HCO_3^- and SO_4^{2-} should occur. Our work found that although the $Na^+/Ca^{2+}/Cl^-/HCO_3^-/SO_4^{2-}$ combined aging treatment had a certain negative effect on the performance of LMB capping to hinder the release of P from sediment, the A-LMB capping still can be effective in the control of sediment internal phosphorus pollution. Thus, LMB is suitably used as an active capping material to limit the release of internal phosphorus to OW. Sediment resuspension induced by hydrodynamics is frequent in shallow freshwater bodies (Cheng and Hua, 2016; Yang et al., 2023; Yin et al., 2016a). Under the action of strong hydrodynamics, the integrality of LMB capping layer will be destroyed, resulting in the mixing of LMB with sediment. Our research found that the R-LMB and A-LMB addition still can be effective in the inhibition of endogenous P release to OW under anoxia condition, and the inactivation of DGT-UP and PM-P in sediment acted as a key role in the suppression of endogenous P liberation to OW by the R-LMB and A-LMB addition. Therefore, the LMB

capping/addition combined technology, i.e., sediment capping using LMB at first and then gradual mixing of LMB with sediment, is very promising approach for addressing the problem of internal phosphorus release in shallow freshwater bodies where sediment resuspension induced by hydrodynamics often takes place.

4. Conclusions

(1) The combined aging treatment of R-LMB with Na^+, Ca^{2+}, Cl^-, HCO_3^- and SO_4^{2-} can inhibit the adsorption of $H_iPO_4^{i-3}$. The combined aging treatment of R-LMB with Na^+, Ca^{2+}, Cl^-, HCO_3^- and SO_4^{2-} can only have a limited effect on the mechanism for the uptake of $H_iPO_4^{i-3}$, and the precipitation of $H_iPO_4^{i-3}$ with La^{3+} to form $LaPO_4$ and the ligand exchange between CO_3^{2-} and $H_iPO_4^{i-3}$ to form the inner-sphere lanthanum-phosphate complexes are still the important mechanisms for the $H_iPO_4^{i-3}$ uptake by A-LMB.
(2) The R-LMB and A-LMB addition can be effective in the interception of endogenous phosphorus release to OW under hypoxia condition, and the immobilization of DGT-UP and PM-P in sediment acted as a key role in the restraint of endogenous phosphorus release by the R-LMB and A-LMB addition.
(3) The R-LMB and A-LMB capping can effectively prevent the internal phosphorus release to OW under anoxia condition, and the inactivation of DGT-UP and PM-P in the topmost sediment played a key role in the suppression of endogenous phosphorus transport into OW by the R-LMB and A-LMB capping.
(4) The combined aging treatment of LMB with Na^+, Ca^{2+}, Cl^-, HCO_3^- and SO_4^{2-} reduced the efficiencies of LMB addition and capping to restrain the release of internal phosphorus to OW under hypoxia condition in some degree.
(5) LMB has a high potential to be used as a capping/amendment material to control internal phosphorus pollution.

Author contribution

Yanhui Zhan: Project administration; Validation; Supervision; Visualization; Resources; Roles/Writing – original draft; Writing – review & editing; Resources. Bo Qiu: Data curation; Formal analysis; Investigation; Software; Roles/Writing – original draft. Jianwei Lin: Conceptualization; Funding acquisition; Methodology; Roles/Writing – original draft; Writing – review & editing; Resources.

Declaration of competing interest

The authors declare that they have no known competing financial interests or personal relationships that could have appeared to influence the work reported in this paper.

Data availability

No data was used for the research described in the article.

Acknowledgements

This study was financially supported by the National Science Foundation of China (Grant No. 51408354 and 50908142), the Capacity Building Project of Some Local Universities of Shanghai Science and Technology Commission (Grant No. 10230502900 and 20050501600), and the Program for Shanghai Collaborative Innovation Center for Cultivating Elite Breeds and Green-culture of Aquaculture animals (Grant No. 2021-KJ-02-12).

References

Adil, S., Kim, J.-O., 2023. The effectiveness and adsorption mechanism of iron-carbon nanotube composites for removing phosphate from aqueous environments. Chemosphere 313, 137629.
Chen, C., Wang, Y., Pang, X., Long, L., Xu, M., Xiao, Y., Liu, Y., Yang, G., Deng, S., He, J., Tang, H., 2021. Dynamics of sediment phosphorus affected by mobile aeration: pilot-scale simulation study in a hypereutrophic pond. J. Environ. Manag. 297, 113297.
Chen, H., Lu, C., Yang, H., 2020. Lanthanum compounds-modified rectorite composites for highly efficient phosphate removal from wastewater. Appl. Clay Sci. 199, 105875.
Chen, M., Ding, S., Chen, X., Sun, Q., Fan, X., Lin, J., Ren, M., Yang, L., Zhang, C., 2018. Mechanisms driving phosphorus release during algal blooms based on hourly changes in iron and phosphorus concentrations in sediments. Water Res. 133, 153–164.
Chen, M., Ding, S., Liu, L., Xu, D., Gong, M., Tang, H., Zhang, C., 2016. Kinetics of phosphorus release from sediments and its relationship with iron speciation influenced by the mussel (Corbicula fluminea) bioturbation. Sci. Total Environ. 542, 833–840.
Chen, Q., Chen, J., Wang, J., Guo, J., Jin, Z., Yu, P., Ma, Z., 2019. In situ, high-resolution evidence of phosphorus release from sediments controlled by the reductive dissolution of iron-bound phosphorus in a deep reservoir, southwestern China. Sci. Total Environ. 666, 39–45.
Cheng, H., Hua, Z., 2016. Effects of hydrodynamic disturbances and resuspension characteristics on the release of tetrabromobisphenol A from sediment. Environ. Pollut. 219, 785–793.
Copetti, D., Finsterle, K., Marziali, L., Stefani, F., Tartari, G., Douglas, G., Reitzel, K., Spears, B.M., Winfield, I.J., Crosa, G., D'Haese, P., Yasseri, S., Lürling, M., 2016. Eutrophication management in surface waters using lanthanum modified bentonite: a review. Water Res. 97, 162–174.
DeVilbiss, S.E., Steele, M.K., Brown, B.L., Badgley, B.D., 2022. Stream bacterial diversity peaks at intermediate freshwater salinity and varies by salt type. Sci. Total Environ. 840, 156690.
Dithmer, L., Lipton, A.S., Reitzel, K., Warner, T.E., Lundberg, D., Nielsen, U.G., 2015. Characterization of phosphate sequestration by a lanthanum modified bentonite clay: a solid-state NMR, EXAFS, and PXRD study. Environ. Sci. Technol. 49, 4559–4566.
Flower, H., Rains, M., Taşcı, Y., Zhang, J.-Z., Trout, K., Lewis, D., Das, A., Dalton, R., 2022. Why is calcite a strong phosphorus sink in freshwater? Investigating the adsorption mechanism using batch experiments and surface complexation modeling. Chemosphere 286, 131596.
Freundlich, H., 1926. Colloid and Capillary Chemistry. Methuen, London.
Fuchs, E., Funes, A., Saar, K., Reitzel, K., Jensen, H.S., 2018. Evaluation of dried amorphous ferric hydroxide CFH-12® as agent for binding bioavailable phosphorus in lake sediments. Sci. Total Environ. 628–629, 990–996.
Funes, A., del Arco, A., Alvarez-Manzaneda, I., de Vicente, J., de Vicente, I., 2017. A microcosm experiment to determine the consequences of magnetic microparticles application on water quality and sediment phosphorus pools. Sci. Total Environ. 579, 245–253.
Gibbs, M., Özkundakci, D., 2011. Effects of a modified zeolite on P and N processes and fluxes across the lake sediment–water interface using core incubations. Hydrobiologia 661, 21–35.
Gibbs, M.M., Hickey, C.W., Özkundakci, D., 2011. Sustainability assessment and comparison of efficacy of four P-inactivation agents for managing internal phosphorus loads in lakes: sediment incubations. Hydrobiologia 658, 253–275.
Haghseresht, F., Wang, S., Do, D.D., 2009. A novel lanthanum-modified bentonite, Phoslock, for phosphate removal from wastewaters. Appl. Clay Sci. 46, 369–375.
He, Q., Zhao, H., Teng, Z., Wang, Y., Li, M., Hoffmann, M.R., 2022. Phosphate removal and recovery by lanthanum-based adsorbents: a review for current advances. Chemosphere 303, 134987.
Isidoro Ribeiro, N., Barreto Pessanha, O., Luiza Gomes Soares Pessanha, M., Guimarães, D., 2023. Efficient phosphate adsorption by a composite composed of Mg6Al2(CO3)(OH)16·4H2O LDH and Chitosan: kinetic, thermodynamic, desorption, and characterization studies. Sep. Purif. Technol. 307, 122717.
Jiang, S., Wang, J., Qiao, S., Zhou, J., 2021. Phosphate recovery from aqueous solution through adsorption by magnesium modified multi-walled carbon nanotubes. Sci. Total Environ. 796, 148907.
Jiao, Y., Xu, L., Li, Q.M., Gu, S., 2020. Thin-layer fine-sand capping of polluted sediments decreases nutrients in overlying water of Wuhan Donghu Lake in China. Environ. Sci. Pollut. Res. 27, 7156–7165.
Kang, L., Mucci, M., Lürling, M., 2022. Influence of temperature and pH on phosphate removal efficiency of different sorbents used in lake restoration. Sci. Total Environ. 812, 151489.
Khnifira, M., Boumya, W., Attarki, J., Mahsoune, A., Abdennouri, M., Sadiq, M., Kaya, S., Barka, N., 2023. Adsorption characteristics of dopamine by activated carbon: experimental and theoretical approach. J. Mol. Struct. 1278, 134964.
Kim, L.H., Choi, E., Stenstrom, M.K., 2003. Sediment characteristics, phosphorus types and phosphorus release rates between river and lake sediments. Chemosphere 50, 53–61.
Kim, T., Lee, J., Yang, I., Kim, B.-G., Choi, Y.R., Jung, J.C., Na, H.B., 2023. Lanthanum oxide-based nanomaterials synthesized by using carbon aerogel template for efficient phosphate capture. Appl. Surf. Sci. 610, 155424.
Koh, K.Y., Zhang, S., Paul Chen, J., 2020. Hydrothermally synthesized lanthanum carbonate nanorod for adsorption of phosphorus: material synthesis and optimization, and demonstration of excellent performance. Chem. Eng. J. 380, 122153.

Kong, M., Liu, F., Tao, Y., Wang, P., Wang, C., Zhang, Y., 2020. First attempt for in situ capping with lanthanum modified bentonite (LMB) on the immobilization and transformation of organic phosphorus at the sediment-water interface. Sci. Total Environ. 741, 140342.
Kurzbaum, E., Bar Shalom, O., 2016. The potential of phosphate removal from dairy wastewater and municipal wastewater effluents using a lanthanum-modified bentonite. Appl. Clay Sci. 123, 182–186.
Kuster, A.C., Huser, B.J., Thongdamrongtham, S., Patra, S., Padungthon, S., Kuster, A.T., 2023. A model for predicting reduction in mobile phosphorus of lake sediment by aluminum drinking water treatment residuals. Water Res. 232, 119677.
Langmuir, I., 1916. The constitution and fundamental properties of solids and liquids Part I. Solid. J. Am. Chem. Soc. 38, 2221–2295.
Li, S., Lin, Z., Liu, M., Jiang, F., Chen, J., Yang, X., Wang, S., 2020. Effect of ferric chloride on phosphorus immobilization and speciation in Dianchi Lake sediments. Ecotoxicol. Environ. Saf. 197, 110637.
Li, X., Xie, Q., Chen, S., Xing, M., Guan, T., Wu, D., 2019. Inactivation of phosphorus in the sediment of the Lake Taihu by lanthanum modified zeolite using laboratory studies. Environ. Pollut. 247, 9–17.
Li, Y., Shang, J.H., Zhang, C., Zhang, W.L., Niu, L.H., Wang, L.F., Zhang, H.J., 2021. The role of freshwater eutrophication in greenhouse gas emissions: a review. Sci. Total Environ. 768, 144582.
Li, Y., Liu, Y., Wang, H., Zuo, Z., Yan, Z., Wang, L., Wang, D., Liu, C., Yu, D., 2023. In situ remediation mechanism of internal nitrogen and phosphorus regeneration and release in shallow eutrophic lakes by combining multiple remediation techniques. Water Res. 229, 119394.
Liang, W.-X., Wei, Y., Qiao, M., Fu, J.-W., Wang, J.-X., 2023. High-gravity-assisted controlled synthesis of lanthanum carbonate for highly-efficient adsorption of phosphate. Sep. Purif. Technol. 307, 122696.
Lin, J., Fu, Z., Yao, J., Wei, X., Wang, D., Ning, D., Chen, M., 2022. Behavior of iron and other heavy metals in passivated sediments and the coupling effect on phosphorus. Sci. Total Environ. 808, 152151.
Lin, J.A., Fu, Z., Ding, S.M., Ren, M.Y., Gao, S.S., 2021. Laboratory investigation on calcium nitrate induced coupling reactions between nitrogen, phosphorus, sulfur, and metals in contaminated sediments. Environ. Sci. Pollut. Res. 28, 25866–25877.
Lin, J.W., Wang, H., Zhan, Y.H., Zhang, Z., 2016. Evaluation of sediment amendment with zirconium-reacted bentonite to control phosphorus release. Environ. Earth Sci. 75, 942–958.
Liu, Y., Sheng, X., Dong, Y., Ma, Y., 2012. Removal of high-concentration phosphate by calcite: effect of sulfate and pH. Desalination 289, 66–71.
Lürling, M., Oosterhout, F.v., 2013. Controlling eutrophication by combined bloom precipitation and sediment phosphorus inactivation. Water Res. 47, 6527–6537.
Lürling, M., Waajen, G., van Oosterhout, F., 2014. Humic substances interfere with phosphate removal by lanthanum modified clay in controlling eutrophication. Water Res. 54, 78–88.
Meis, S., Spears, B.M., Maberly, S.C., O'Malley, M.B., Perkins, R.G., 2012. Sediment amendment with Phoslock® in Clatto Reservoir (Dundee, UK): investigating changes in sediment elemental composition and phosphorus fractionation. J. Environ. Manag. 93, 185–193.
Moumen, E., Bazzi, L., El Hankari, S., 2022. Aluminum-fumarate based MOF: a promising environmentally friendly adsorbent for the removal of phosphate. Process Saf. Environ. 160, 502–512.
Mucci, M., Douglas, G., Lürling, M., 2020. Lanthanum modified bentonite behaviour and efficiency in adsorbing phosphate in saline waters. Chemosphere 249, 126131.
Norgbey, E., Li, Y., Ya, Z., Li, R., Nwankwegu, A.S., Takyi-Annan, G.E., Luo, F., Jin, W., Huang, Y., Sarpong, L., 2020. High resolution evidence of iron-phosphorus-sulfur mobility at hypoxic sediment water interface: an insight to phosphorus remobilization using DGT-induced fluxes in sediments model. Sci. Total Environ. 724, 138204.
Paytan, A., Roberts, K., Watson, S., Peek, S., Chuang, P.-C., Defforey, D., Kendall, C., 2017. Internal loading of phosphate in lake erie central basin. Sci. Total Environ. 579, 1356–1365.
Reitzel, K., Andersen, F.Ø., Egemose, S., Jensen, H.S., 2013. Phosphate adsorption by lanthanum modified bentonite clay in fresh and brackish water. Water Res. 47, 2787–2796.
Reitzel, K., Balslev, K.A., Jensen, H.S., 2017. The influence of lake water alkalinity and humic substances on particle dispersion and lanthanum desorption from a lanthanum modified bentonite. Water Res. 125, 191–200.
Rezania, S., Kadi, A., Kamyab, H., Ghfar, A.A., Rashidi Nodeh, H., Wan Ibrahim, W.N., 2022. Lanthanum doped magnetic polyaniline for removal of phosphate ions from water. Chemosphere 307, 135809.
Ross, G., Haghseresht, F., Cloete, T.E., 2008. The effect of pH and anoxia on the performance of Phoslock®, a phosphorus binding clay. Harmful Algae 7, 545–550.
Rydin, E., 2000. Potentially mobile phosphorus in Lake Erken sediment. Water Res. 34, 2037–2042.
Rydin, E., Welch, E.B., 1998. Aluminum dose required to inactivate phosphate in lake sediments. Water Res. 32, 2969–2976.
Schindler, D.W., Carpenter, S.R., Chapra, S.C., Hecky, R.E., Orihel, D.M., 2016. Reducing phosphorus to curb lake eutrophication is a success. Environ. Sci. Technol. 50, 8923–8929.
Schindler, D.W., Hecky, R.E., Findlay, D.L., Stainton, M.P., Parker, B.R., Paterson, M.J., Beaty, K.G., Lyng, M., Kasian, S.E.M., 2008. Eutrophication of lakes cannot be controlled by reducing nitrogen input: results of a 37-year whole-ecosystem experiment. Proc. Natl. Acad. Sci. USA 105, 11254–11258.
Sills, J., Schelske, C.L., 2009. Eutrophication: focus on phosphorus. Science 324, 722-722.
Sondergaard, M., Jensen, J.P., Jeppesen, E., 2003. Role of sediment and internal loading of phosphorus in shallow lakes. Hydrobiologia 506, 135–145.
Sun, B., Chen, W., Li, N., Wang, W., Fu, C., Liu, Y., Gao, X., 2022. Quantifying the effects of submerged aquatic vegetation on internal loading in lake: a modeling study of the largest shallow lake in North China. Sci. Total Environ. 853, 158593.
Tammeorg, O., Nürnberg, G.K., Tõnno, I., Kisand, A., Tuvikene, L., Nõges, T., Nõges, P., 2022. Sediment phosphorus mobility in Võrtsjärv, a large shallow lake: insights from phosphorus sorption experiments and long-term monitoring. Sci. Total Environ. 829, 154572.
Tran, H.N., You, S.-J., Hosseini-Bandegharaei, A., Chao, H.-P., 2017. Mistakes and inconsistencies regarding adsorption of contaminants from aqueous solutions: a critical review. Water Res. 120, 88–116.
Van Heyst, A., A S., Jamieson, R., 2022. Application of phosphorus loading models to understand drivers of eutrophication in a complex rural lake-watershed system. J. Environ. Manag. 302, 114010.
Wang, C., Liang, J., Pei, Y., Wendling, L.A., 2013. A method for determining the treatment dosage of drinking water treatment residuals for effective phosphorus immobilization in sediments. Ecol. Eng. 60, 421–427.
Wang, J., Chen, J., Yu, P., Yang, X., Zhang, L., Geng, Z., He, K., 2020. Oxygenation and synchronous control of nitrogen and phosphorus release at the sediment-water interface using oxygen nano-bubble modified material. Sci. Total Environ. 725, 138258.
Wang, Y., Ding, S.M., Wang, D., Sun, Q., Lin, J., Shi, L., Chen, M.S., Zhang, C.S., 2017. Static layer: a key to immobilization of phosphorus in sediments amended with lanthanum modified bentonite (Phoslock®). Chem. Eng. J. 325, 49–58.
Watson, S.B., Miller, C., Arhonditsis, G., Boyer, G.L., Carmichael, W., Charlton, M.N., Confesor, R., Depew, D.C., Höök, T.O., Ludsin, S.A., Matisoff, G., McElmurry, S.P., Murray, M.W., Peter Richards, R., Rao, Y.R., Steffen, M.M., Wilhelm, S.W., 2016. The re-eutrophication of Lake Erie: harmful algal blooms and hypoxia. Harmful Algae 56, 44–66.
Wu, D., Zhan, Y., Lin, J., Zhang, Z., Xie, B., 2022. Contrasting effect of lanthanum hydroxide and lanthanum carbonate treatments on phosphorus mobilization in sediment. Chem. Eng. J. 427, 132021.
Xia, L., Verbeeck, M., Bergen, B., Smolders, E., 2023. Effect of external and internal loading on source-sink phosphorus dynamics of river sediment amended with iron-rich glauconite sand. J. Environ. Manag. 332, 117396.
Xu, T., Yang, T., Xiong, M.L., 2020. Time scales of external loading and spatial heterogeneity in nutrients-chlorophyll a response: implication on eutrophication control in a large shallow lake. Ecol. Eng. 142, 105636.
Yang, C., Wang, G., Yin, H., 2023. Response of internal phosphorus loading from dredged and inactivated sediment under repeated resuspension in a eutrophic shallow lake. Sci. Total Environ. 868, 161653.
Yang, C., Yang, P., Geng, J., Yin, H., Chen, K., 2020. Sediment internal nutrient loading in the most polluted area of a shallow eutrophic lake (Lake Chaohu, China) and its contribution to lake eutrophication. Environ. Pollut. 262, 114292.
Yang, M.J., Lin, J.W., Zhan, Y.H., Zhu, Z.L., Zhang, H.H., 2015. Immobilization of phosphorus from water and sediment using zirconium-modified zeolites. Environ. Sci. Pollut. Res. 22, 3606–3619.
Yang, S., Wang, Q., Zhao, H., Liu, D., 2022a. Bottom-up synthesis of MOF-derived magnetic Fe-Ce bimetal oxide with ultrahigh phosphate adsorption performance. Chem. Eng. J. 448, 137627.
Yang, Y., Wang, Y., Zheng, C., Lin, H., Xu, R., Zhu, H., Bao, L., Xu, X., 2022b. Lanthanum carbonate grafted ZSM-5 for superior phosphate uptake: investigation of the growth and adsorption mechanism. Chem. Eng. J. 430, 133166.
Yang, X.N., Zhong, M., Pu, J., Liu, C.Z., Luo, H., Xu, M.Y., 2022. Risk control and assessment of sulfide-rich sediment remediation by controlled-release calcium nitrate. Water Res. 226, 119230.
Yang, Y., Zhu, H., Xu, X., Bao, L., Wang, Y., Lin, H., Zheng, C., 2021. Construction of a novel lanthanum carbonate-grafted ZSM-5 zeolite for effective highly selective phosphate removal from wastewater. Microporous Mesoporous Mater. 324, 111289.
Yin, H., Kong, M., 2015. Reduction of sediment internal P-loading from eutrophic lakes using thermally modified calcium-rich attapulgite-based thin-layer cap. J. Environ. Manag. 151, 178–185.
Yin, H., Kong, M., Fan, C., 2013. Batch investigations on P immobilization from wastewaters and sediment using natural calcium rich sepiolite as a reactive material. Water Res. 47, 4247–4258.
Yin, H., Kong, M., Han, M., Fan, C., 2016a. Influence of sediment resuspension on the efficacy of geoengineering materials in the control of internal phosphorous loading from shallow eutrophic lakes. Environ. Pollut. 219, 568–579.
Yin, H., Ren, C., Li, W., 2018. Introducing hydrate aluminum into porous thermally-treated calcium-rich attapulgite to enhance its phosphorus sorption capacity for sediment internal loading management. Chem. Eng. J. 348, 704–712.
Yin, H., Zhang, M., Yin, P., Li, J., 2022a. Characterization of internal phosphorus loading in the sediment of a large eutrophic lake (Lake Taihu, China). Water Res. 225, 119125.
Yin, H.B., Han, M.X., Tang, W.Y., 2016b. Phosphorus sorption and supply from eutrophic lake sediment amended with thermally-treated calcium-rich attapulgite and a safety evaluation. Chem. Eng. J. 285, 671–678.
Yin, X., Li, X., Petropoulos, E., Feng, Y., Yang, B., Xue, L., Yang, L., He, S., 2022b. Phosphate removal from actual wastewater via La(OH)3-C3N4 adsorption: performance, mechanisms and applicability. Sci. Total Environ. 814, 152791.
Yu, J., Zeng, Y., Chen, J., Liao, P., Yang, H., Yin, C., 2022. Organic phosphorus regeneration enhanced since eutrophication occurred in the sub-deep reservoir. Environ. Pollut. 306, 119350.

Zamparas, M., Gavriil, G., Coutelieris, F.A., Zacharias, I., 2015. A theoretical and experimental study on the P-adsorption capacity of Phoslock. Appl. Surf. Sci. 335, 147–152.
Zang, N., Zhu, J., Wang, X., Liao, Y., Cao, G., Li, C., Liu, Q., Yang, Z., 2022. Eutrophication risk assessment considering joint effects of water quality and water quantity for a receiving reservoir in the South-to-North Water Transfer Project, China. J. Clean. Prod. 331, 129966.
Zhan, Y., Yu, Y., Lin, J., 2020. Impact of application mode on the control of phosphorus release from sediments using zirconium-modified bentonite as geo-engineering material. Sci. Total Environ. 712, 135633.
Zhan, Y.H., Chang, M.Y., Lin, J.W., 2021. Suppression of phosphorus release from sediment using lanthanum carbonate as amendment. Environ. Sci. Pollut. Res. 28, 3280–3295.
Zhang, C., Wang, X., Wang, X., Liu, B., 2022. Characterization of La–Mg-modified palygorskite and its adsorption of phosphate. J. Environ. Chem. Eng. 10, 107658.
Zhang, H., Davison, W., Gadi, R., Kobayashi, T., 1998. In situ measurement of dissolved phosphorus in natural waters using DGT. Anal. Chim. Acta 370, 29–38.
Zhang, H., Davison, W., Miller, S., Tych, W., 1995. In situ high resolution measurements of fluxes of Ni, Cu, Fe, and Mn and concentrations of Zn and Cd in porewaters by DGT. Geochem. Cosmochim. Acta 59, 4181–4192.
Zhang, H., Lyu, T., Liu, L., Hu, Z., Chen, J., Su, B., Yu, J., Pan, G., 2021. Exploring a multifunctional geoengineering material for eutrophication remediation: simultaneously control internal nutrient load and tackle hypoxia. Chem. Eng. J. 406, 127206.
Zheng, Y., Sun, Y., Zhang, Z., Han, C., Wang, Z., Liu, C., Ke, F., Zhang, L., Shen, Q., 2023. Evaluation of the distribution and mobility of labile phosphorus in sediment profiles of Lake Nansi, the largest eutrophic freshwater lake in northern China. Chemosphere 315, 137756.
Zhong, Z., Lu, X., Yan, R., Lin, S., Wu, X., Huang, M., Liu, Z., Zhang, F., Zhang, B., Zhu, H., Guo, X., 2020. Phosphate sequestration by magnetic La-impregnated bentonite granules: a combined experimental and DFT study. Sci. Total Environ. 738, 139636.
Zhou, J., Li, D., Zhao, Z., Huang, Y., 2021. Phosphorus bioavailability and the diversity of microbial community in sediment in response to modified calcium peroxide ceramsite capping. Environ. Res. 195, 110682.